

# **Egyptian Journal of Chemistry**

http://ejchem.journals.ekb.eg/



# White Bean Straw-Derived Biosorbent for Efficient Removal of Cationic and Anionic Dyes: A Sustainable Approach to Agricultural Waste Valorization



Amany G. Abo-Mousa<sup>1,2,\*</sup>, Marwa M. Abdeen<sup>1</sup>, Safaa R. Fouda<sup>1,3</sup>, Mamdouh A. Gadalla<sup>4,5</sup>, Rehab M. El-Maghraby<sup>6</sup>, Ayat O. Ghallab<sup>2,7</sup>, Mai K. Fouad<sup>2</sup>

<sup>1</sup>Higher Institute of Engineering and Technology, Chemical Engineering Department, Menofia, 32821, Egypt.

<sup>2</sup>Cairo University, Chemical Engineering Department, Cairo, 12613, Egypt

<sup>3</sup>Ain Shams University, Chemistry Department, Abbassia, 11566, Egypt.

<sup>4</sup>Port Said University, Chemical Engineering Department, Port Said, 42526, Egypt.

<sup>5</sup>Faculty of Engineering and the Built Environment, University of the Witwatersrand, Johannesburg, South Africa.

<sup>6</sup>Petroleum Refinery and Petrochemical Engineering Department, Faculty of Petroleum and Mining Engineering, Suez University, Suez, Egypt.

<sup>7</sup> School of Energy and Environmental Engineering, Nile University, 12588 Giza, Egypt.

#### Abstract

White bean straw (WBS), a low-cost, locally available agricultural waste, was used as a biosorbent for the adsorption of Malachite Green, Alizarin Red S, and Methyl Red dyes. Characterization using scanning electron microscopy, infrared spectroscopy, zeta potential analyzer, and X-ray diffractometer showed that the surface is coarse and heterogeneous, and detected functional groups essential for effective adsorption. It was also noted that carbon and oxygen are the primary components of White bean straw. White bean straw is a highly effective adsorbent material for removing both cationic and anionic dyes, as it exhibits two points of zero charge (1.7 and 10.8). The effects of particle size, contact time, dosage, solution pH, temperature, and initial dye concentration on the removal efficiency of each dye by WBS were investigated. It was found that the models that best fit the Methyl Red (MR), Alizarin Red S (ARS), and Malachite Green (MG) dyes were the pseudo-second-order adsorption kinetics and the Freundlich adsorption isotherm models. The removal efficiency reached approximately 95.7%, 61.2% and 98.2% for MR, ARS, and MG, respectively. Physical adsorption is indicated by values of -62.311 J/mol. K. and -81.358 J/mol. K. for MR and ARS, while chemisorption is indicated by values of -227.37 J/mol. K. for MG. The adsorption process is exothermic and largely dependent on electrostatic contact, since enthalpy is negative for each dye. For MR, ARS, and MG, the process is spontaneous because Gibbs free energy is negative for all at 25°C, 35°C, and 45°C.

Keywords: White bean straw; biosorbents; cationic dye; anionic dye; azo dye.

# 1. Introduction

While industrial advancements have greatly enhanced production capacity and improved the quality of life, they have also led to significant environmental concerns, particularly the release of hazardous synthetic chemicals and dyes [1, 2]. The widespread use of synthetic dyes in textiles, paper, cosmetics, printing, food processing, leather, wool, and plastics presents serious ecological and health risks. Among various industrial pollutants, textile wastewater is a primary source of water contamination [3].

Dyes fall into two main categories: natural and synthetic. Natural dyes are derived from plants, animals, or minerals, while synthetic dyes, offering a broader color range and greater stability, are produced through chemical synthesis. Synthetic dyes are further categorized into various classes, such as acid, basic, reactive, vat, and dispersed dyes, each designed for specific materials like cotton, wool, silk, or synthetic Fibers. While essential in industries, dyes pose significant environmental and health risks. Certain classes, like azo dyes, are particularly concerning due to their toxicity and persistence in wastewater, leading to oxygen depletion, aquatic life suffocation, and disrupted ecosystems [4]. Even at concentrations below 1 ppm, dyes can visibly alter water quality, prevent light penetration, and harm aquatic plants. Additionally, many dyes are carcinogenic, mutagenic, and hazardous to both humans and animals, making their removal from wastewater crucial for environmental and public health [5].

The treatment of dye-contaminated wastewater is essential before its release into the environment due to its harmful environmental and health effects [6]. Recently, various methods have been devised to address dye contamination, encompassing physical, chemical, and biological approaches, including electrocoagulation, flotation, photocatalysis,

\*Corresponding author e-mail: <a href="mailto:amanyg910@gmail.com">amanyg910@gmail.com</a>.; (Amany G. Abo-Mousa). Received Date: 31 May 2025, Revised Date: 29 July 2025, Accepted Date: 26 August 2025

DOI: 10.21608/EJCHEM.2025.390539.11845

©2026 National Information and Documentation Center (NIDOC)

flocculation, ozonation, and membrane filtration [7]. Among the various removal techniques, adsorption is widely recognized as one of the most effective methods due to its simplicity, safety, high effectiveness, ease of application, and cost efficiency [8].

Adsorbents can originate from various biomass sources, such as grass waste, walnut shells, fungi, berry seeds, rice husk, and algal waste, or industrial byproducts like red mud and fly ash [9]. While industrial alternatives may pose additional contamination risks, biomass-derived adsorbents (biosorbents) only require pretreatment to enhance their efficiency. They have the advantage of offering a cost-effective and widely available solution, requiring only basic processing steps such as washing and milling [10]. Waste biomass is frequently baled for animal feed, but there is often excess beyond this demand. In this research, white bean straw (WBS) is employed to remove certain dyes, highlighting the potential of agricultural residues as sustainable and economical biosorbents, particularly since vegetable harvesting and processing result in around 30% (w/w) waste [11].

#### 2. Literature Review

Numerous promising biosorbent materials have been explored in the literature for dye removal from wastewater. Babalola et al. utilized Cedrela odorata seeds to eliminate methylene blue, Congo red, methyl orange, and crystal violet from aqueous effluents [12], while Georgin et al. applied Araucaria angustifolia wastes for the treatment of crystal violet-contaminated effluents [13]. Carvalho et al. tested activated carbon derived from jerivá stone [14], and Postai et al. employed Aleurites moluccana residues for the removal of rhodamine B from aqueous solutions [11]. Dávila-Jiménez et al. investigated the use of mango rock for eliminating anthraquinone and azo dyes [15], whereas Fontana et al. applied malt bagasse as a cost-effective biosorbent for textile dye removal [16]. Additionally, Munagapati et al. demonstrated the efficiency of banana peel powder in removing reactive black 5 and Congo red from aqueous solutions [17].

Alkaline-modified walnut shells have been employed by Halysh et al. [18] for the removal of methylene blue. Similarly, agro-food waste like dried watermelon peels has been utilized as a natural biosorbent to eliminate Acid Blue 193 (AB193) and Acid Orange 95 (AO95) from aqueous solutions [19]. Additionally, agricultural by-products such as peanut shells (PS) and corn cobs (CC) have been applied as eco-friendly adsorbents for the removal of Reactive Red 43 (RR43) [20]. These studies highlight the ongoing pursuit of sustainable, low-cost biosorbents as viable solutions for treating textile effluents.

Most studies have focused on either cationic or anionic dyes; however, textile wastewater is typically complicated, and adsorption with a single ionic group type is normally unable to remove different ionic dyes.

This study aims to evaluate the potential of white bean straw (WBS) as an effective, low-cost biosorbent for the removal of different synthetic dyes from aqueous solutions. It investigates the adsorption behavior of WBS toward various dye types, including Malachite Green (MG), Alizarin Red S (ARS), and Methyl Red (MR), under varying conditions such as pH, contact time, adsorbent dosage, temperature, dye concentration, and particle size. In addition, the raw and dye-loaded biosorbent materials are characterized using FTIR, SEM, and EDX analyses to examine surface functional groups, morphology, and elemental composition before and after adsorption. It is hypothesized that WBS will exhibit enhanced adsorption performance due to its surface properties, allowing efficient interaction with different dye molecules through mechanisms such as electrostatic attraction, hydrogen bonding, and  $\pi$ - $\pi$  interactions.

# 3. Materials and Methods

# 3.1. Adsorbent preparation

White Bean Straw was gathered from fields in the Menoufia region of Egypt following the white bean harvest season. Tap water and distilled water were used to wash the sample twice to remove the contaminants [21]. After being dried at 105°C, the straw was allowed to dry in air, then milled into a powder with varying particle sizes.

#### 3.2. Adsorbate preparation

A stock solution was made by dissolving one gram of the applied dye in one liter of distilled water. To create the experimental solutions at the necessary concentration, the stock solution was subsequently diluted with distilled water. The properties and molecular structure of these dyes are shown in Table 1.

Table 1: General characteristics of Malachite Green (MG), Methyl Red (MR), and Alizarin Red S(ARS) (Sigma-Aldrich, 2012)

Common Name	Chemical Structure	Empirical Formula	C.I. number	Molecular Weight (g/mol)	Wavelength(n m)
Malachite Green (MG)	CI-	C <sub>23</sub> H <sub>25</sub> ClN <sub>2</sub>	42000	364.9 g/mol	618

#### 3.3. Characterization of the as-designed White Bean Straw biosorbents

An X-ray diffractometer was used to examine the biosorbent structure of White Bean Straw (WBS) using Cu K- $\alpha$  radiation ( $\lambda$ =1.5418 Å) and a scanning rate of 0.3 degrees per minute. At Altabyin Research Institute, X-ray diffraction (XRD) study within a 20 range of 5–70 helped in clarifying the crystallinity of the biosorbents. The JSM 7500 FA (Japan) High Resolution Cold Field Emission was utilized in conjunction with scanning electron microscopy (SEM) to display the samples' microscopic morphologies. SEM images and energy-dispersive X-ray analysis (EDX) were acquired to examine the materials' composition. Tanta Central Laboratory performed the analysis of Fourier transform Infrared Spectroscopy (FT-IR) spectra. Using a Shimazu UV-2450 and a KBr disk for recording, the JASCO spectrophotometer type FT/IR-4100 was operated in the wave number range of 4000 to 400 cm-1. A zeta potential analyzer (Malvern Instruments Co. Ltd., United Kingdom) was used to perform zeta potential measurements. The electrolyte solution was 10-3M KCl, and the pH regulators were 0.1N HCl and NaOH solutions, to measure the particle surface charge.

#### 3.4. Batch Adsorption Experiment

Batch experiments were performed to find the optimal conditions for the equilibrium adsorption of the three colors onto WBS. Since flocculation, oxidation, and membrane separation all require high pressures and typically result in sludge, batch adsorption was selected for its dependability and simplicity of use [22]. The impact of initial dye concentration, residence period, dosage, solution pH and temperature, and particle size was examined.

The batch adsorption process in water treatment typically involves several key steps. First, a known quantity of adsorbent, WBS, is added to a predetermined volume of contaminated water with dyes. The mixture is then stirred or agitated to ensure adequate contact between the adsorbent and the dyes. This is followed by a specified contact time during which the dyes are adsorbed onto the surface of the adsorbent. Once the material has reached adsorption equilibrium, the treated water is separated from the adsorbent, often through filtration. The filtrate was examined at each dye's maximum absorbance wavelength using a Perkin-Elmer UV-visible spectrophotometer. Depending on the results, the process may be adjusted by altering parameters like adsorbent dosage, contact time, or water temperature to improve treatment performance. This batch process provides flexibility in treating water samples, allowing for optimization of the adsorbent's effectiveness in removing specific pollutants [23]. The quantity of contamination that can be adsorbed per unit mass of the adsorbent material's surface is known as its adsorption capacity. –Eq.1 may be used to determine the adsorption capacity (qe), and Eq.2 can be used to express the adsorption removal efficiency.

$$(q_c) = \frac{(C_0 - C_c) \times V}{m} \tag{1}$$

$$R(\%) = \left(\frac{C_0 - C_e}{C_0}\right) \times 100$$
(2)

Where  $q_e$  is the adsorption capacity (mg/g), m is the mass of the adsorbent (g), V is the volume of dye solution (L), and Co and Ce are the initial and final equilibrium concentrations (mg/L) of dye in solution, respectively [24].

#### 3.4.1. Absorbance and concentration calibration curve

A calibration curve using UV-Vis spectroscopy at specific wavelengths was created to correlate dye concentration with UV light absorbance, allowing for the conversion of absorbance values into concentrations. UV-Vis was used to assess known concentrations of MG, MR, and ARS at absorbance wavelengths of 618 nm, 520 nm, and 526 nm, respectively.

# 3.4.2. The impact of solution pH on biosorption

0.05 g of less than 150 μm WBS was combined with 15 mL of a 25 mg/L dye solution. The solution's pH was adjusted to 2, 4, 6, 8, 10, and 12 using solutions of sodium hydroxide and hydrochloric acid. For three hours at room temperature, the mixture was agitated at 120 rpm. The absorbance of the dye after removal was measured using UV-Vis.

#### 3.4.3. The impact of starting concentration on biosorption

15 mL of 5, 10, 25, 50, 100, 150, and 200 mg/L solutions at optimum pH of 8 for MG and MR and 10 for ARS were mixed with 0.05 g of less than 150  $\mu$ m WBS. The solutions were stirred at 120 rpm for 3 hours at room temperature. To determine the amount of dye eliminated, the solutions were filtered and subjected to UV-Vis analysis.

#### 3.4.4. The impact of contact time on biosorption

The maximum removal reached for each dye was at 10 mg/L for MG, 100 mg/L for MR, and 25 mg/L for ARS.15 mL of optimal concentration at pH 8 for MG and MR, and 10 for ARS were mixed with 0.05 g of less than  $150 \mu m$  WBS, and stirred at 120 rpm. The solution was filtered every 15 minutes for 3 hours. UV-Vis analysis was used to determine the amount of dye removed.

#### 3.4.5. The impact of WBS size particle on biosorption

After milling, WBS was sieved with 2 mesh sizes: 300  $\mu$ m and 150  $\mu$ m. 15 mL of the optimal concentration of each solution for the three dyes at optimum pH was mixed with 0.05 g of the variously sized WBS (> 300  $\mu$ m, 300–150  $\mu$ m, and < 150  $\mu$ m), and the mixture was stirred at 120 rpm for two hours, as the maximum removal efficiency achieved after two hours. The solution was filtered out of solids, UV-Vis was used for analysis.

#### 3.4.6. The impact of WBS dosage on biosorption

The proper dose of biosorbent is crucial for wastewater treatment. The influence of adsorbent dose was examined at a mass range from 0.01 to 0.1 g of less than  $150 \, \mu m$  WBS.  $15 \, mL$  of optimal concentration ( $10 \, mg/L$  for MG,  $100 \, mg/L$  for MR, and  $25 \, mg/L$  for ARS) at pH 8 for MG and MR, and 10 for ARS were mixed with  $0.01 \, g$ ,  $0.05 \, g$ , and  $0.1 \, g$  of WBS and stirred at  $120 \, rpm$  for  $2 \, hours$ . After the solids were removed from the solution, UV-Vis was employed to analyze it.

#### 3.4.7. The impact of solution temperature on biosorptio

Adsorption was applied at 25°C, 35°C, and 45°C to investigate the effect of temperature. 0.05 g of less than 150 µm WBS were added to 15 mL of dye solution at optimal concentration (10 mg/L for MG, 100 mg/L for MR, and 25 mg/L for ARS) and stirred for 2 hours. After the solution's solids were removed, UV-Vis was utilized to analyze it.

#### 3.5. Equilibrium Isotherms and Kinetics

The adsorption isotherms were examined with starting dye concentrations of 5, 10, 25, 50, 100, 150, and 200 mg/L. The kinetic investigation involved using concentrations of 10 mg/L MG, 100 mg/L MR and 25 mg/L ARS. The optimal pH for dye solutions removal is 8 for MG and MR, and 10 for ARS. These solutions were agitated with 0.05 g of less than 150 µm WBS biosorbent at room temperature for specified intervals (every 15 minutes for 3 hours). A thermostatic shaker operating at 120 rpm was employed to attain equilibrium at room temperature. Samples were filtered, and the remaining dye concentration was measured using a UV–Vis spectrometer.

#### 3.5.1. Model validity

Identifying the most suitable models requires more than just relying on the correlation coefficient (R²); it also necessitates employing additional methods to assess model validity [22]. The model's accuracy was assessed using the sum of squared errors (SSE) and the root mean square error (RMSE) [19, 22]. SSE was determined using Eq. 3:

$$SSE = \sum (q_{exp} - q_{cal})^2 \tag{3}$$

Where adsorption from experimental trials is denoted by  $q_{exp}$ , and adsorption from kinetic or isotherm studies is denoted by  $q_{cal}$ .

Eq. 4 was used to determine RMSE.

$$RMSE = \sqrt{\frac{SSE}{N}}$$
 (4)

Where N is the number of data points.

The best-fitting model will be identified by having the lowest SEE and RMSE values and an R<sup>2</sup> value that is closest to 1.0.

#### 4. Results and discussion

4.1. White Bean Straw (WBS) Characterization

4.1.1. FT-IR measurement results

The functional groups on the WBS biosorbent were characterized using FT-IR spectroscopy, and their interactions with MG, ARS, and MR Dyes (Fig. 1).

The FTIR spectrum provides valuable insight into the main structural components of WBS. The observed absorption bands reflect the presence of cellulose, hemicellulose, and lignin—typical of lignocellulosic agricultural biomass.

The IR spectrum for WBS biosorbent displayed the absorption bands (-OH) group at 3332 cm<sup>-1</sup>, which are commonly found in cellulose, hemicellulose, and lignin. The broad nature of the peak may indicate overlapping with amine (-NH) stretching vibrations. The peaks at 2915 and 1731 cm<sup>-1</sup> are attributed to aliphatic C-H stretching and (C=O) vibration of the carbonyl group, respectively. The peak at 1617 cm<sup>-1</sup> corresponds to the stretching vibrations of aromatic C=C bonds, indicating the presence of lignin. The peak at 1033 cm<sup>-1</sup> is assigned to the (C-O-C) stretching vibration bond in polysaccharides, confirming the presence of cellulose and hemicellulose. Additionally, this region may also contain contributions from Si-O

stretching vibrations, indicating the presence of silicate-based compounds as detected in the Energy Dispersive X-ray (EDX) analysis.

FTIR analysis was performed before and after dye adsorption; The relative intensity of some bands, the formation and disappearance of valleys, and the shift of wavenumbers for particular bands are all displayed in Fig. 1. For WBS/MG, the observed shifts in key functional groups after adsorption indicate successful interaction between the biosorbent and Malachite Green, confirming its effectiveness in dye removal. The shift in the hydroxyl (-OH) peak from 3332 cm<sup>-1</sup> to 3310 cm<sup>-1</sup> suggests hydrogen bonding with the dye molecules. The C=C stretching at 1617 cm<sup>-1</sup> shifted to 1625 cm<sup>-1</sup>, indicating possible interaction between the aromatic rings of Malachite Green and lignin components due to  $\pi$ - $\pi$  interactions. Additionally, the C-O-C stretching at 1032 cm<sup>-1</sup> shifted to 1028 cm<sup>-1</sup>, suggesting changes in polysaccharide structures due to adsorption. The appearance of new peaks at 2330 cm<sup>-1</sup> & 2033 cm<sup>-1</sup> supports the chemical interaction between the biosorbent and nitrogen-containing functional groups of MG dye molecules. Peak at 1340.54 cm<sup>-1</sup> corresponds to C-N stretching vibrations in MG dye, supporting dye adsorption.

For WBS/MR, several spectral changes were observed, indicating interactions between the dye and the biosorbent. A new peak at 1430 cm<sup>-1</sup> appeared. These peaks suggest interactions involving nitrogen-containing functional groups of MR dye, possibly related to azo (-N=N-) bonds. Shift in the peak at 1613 cm<sup>-1</sup>. This band corresponds to C=C stretching vibrations in aromatic rings. The shift suggests interaction between the aromatic rings of Methyl Red and the biosorbent surface, likely through  $\pi$ - $\pi$  interactions. Peak at 1241 cm<sup>-1</sup> may correspond to C-N stretching vibrations, indicating the presence of amine interactions from Methyl Red.

For WBS/ARS, notable spectral shifts were observed, indicating interactions between the dye and the biosorbent. Shifts in the peaks at 1731.10 cm<sup>-1</sup> and 1626.40 cm<sup>-1</sup> correspond to the C=O stretching vibrations of carboxyl (-COOH) groups and the C=C stretching vibrations in aromatic rings, respectively. Their shifts suggest the involvement of these functional groups in the adsorption process, likely through hydrogen bonding, electrostatic interactions, or  $\pi$ - $\pi$  stacking with Alizarin Red S. Peak at 1447.21 cm<sup>-1</sup> likely attributed to C-O stretching vibrations. This peak indicates the participation of phenolic or carboxyl functional groups in the adsorption process. Appearance of a new peak at 539.46 cm<sup>-1</sup> corresponds to C-S bending vibrations, further supporting the adsorption of Alizarin Red S onto the biosorbent

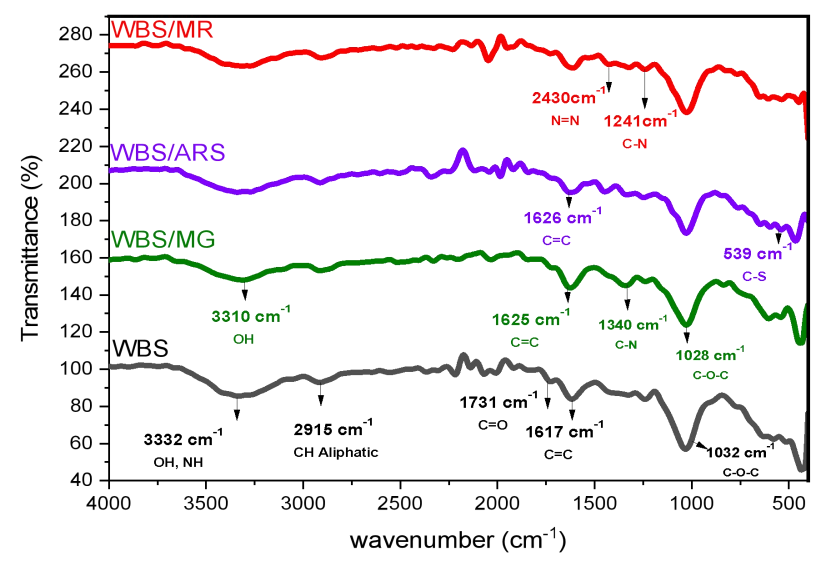


Fig.1. FT-IR spectra of raw White Bean Straw (WBS) biosorbents before and after adsorption of Malachite Green (MG), Methyl Red (MR), and Alizarin Red S (ARS) dyes.

#### 4.1.2. XRD analysis

The XRD pattern of the WBS biosorbents is displayed in Fig. 2. The broad diffraction feature between  $20^{\circ}$  and  $30^{\circ}$  ( $2\theta$ ) suggests that the material is predominantly amorphous, which is characteristic of lignocellulosic biomass. The peak centered around  $21-23^{\circ}$  ( $2\theta$ ) may correspond to amorphous silica ( $SiO_2$ ), as reported for similar agricultural residues [26]. Additional peaks at  $15.42^{\circ}$ ,  $26.23^{\circ}$ ,  $31.73^{\circ}$ , and  $39.49^{\circ}$  indicate the presence of semi-crystalline or crystalline components, possibly due to residual inorganic minerals or organized cellulose regions [27].

The wide hump within 20°–30° may also be attributed to disordered carbonaceous structures formed during the preparation or partial carbonization of the biosorbent, in agreement with literature on biomass-based adsorbents [28], [29].

The crystal size was evaluated according to Scherer's equation [30] as shown in Eq. 5.  $D = \frac{0.9 \lambda}{\beta \cos \theta}$ 

Where D is the crystal size ( $\mu$ m),  $\lambda$  is the X-ray wavelength of x-ray  $\approx 1.541$  Å, and is the full width at half maximum (FWHM). The crystal size is 1.103  $\mu$ m.

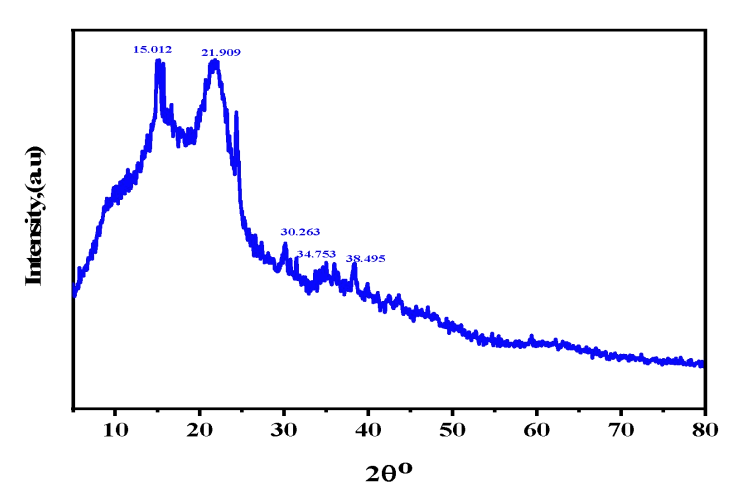
(5)

C-O stretching /

phenolic groups

Functional group / Vibration	WBS (Before) (cm <sup>-1</sup> )	After MG (cm <sup>-1</sup> )	After MR (cm <sup>-1</sup> )	After ARS (cm <sup>-1</sup> )	Interpretation / Notes
-OH stretching	3332	3310	_	_	Shift → H-bonding with dye molecules
C-H aliphatic stretching	2915	_	_	_	No major shift noted
C=O (carbonyl) stretching	1731	_	_	1718	Interaction via hydrogen bonding or electrostatics
C=C aromatic stretching	1617	1625	1613	1626	$\pi$ – $\pi$ interaction with dye aromatic rings
C-N stretching	_	1340	1241	_	Indicates amine group interactions
C-O-C stretching (polysaccharides)	1033	1028	_	_	Slight shift → involvement in adsorption
New peaks	_	2330, 2033	1430	539	New functional groups appearing post-adsorption
C_O stretching /					Involvement of

Table 2: FTIR Peak Shifts of WBS Before and After Dye Adsorption



1447

phenolic/carboxyl

groups

Fig. 2. XRD patterns of raw WBS biosorbents before adsorption.

4.1.3. Scanning Electron Microscopy combined with Energy Dispersive X-Ray Analysis (SEM-EDX Analysis)

The surface morphology of WBS biosorbent was analyzed using SEM-EDX before and after adsorption of MG, ARS, and MR dyes. As shown in Fig. 3a, the elongated fibrous structures seen in the picture indicate the existence of cellulose and lignocellulosic fibers, prevalent in plant-derived biomass. The biosorbent exhibits a rough and fibrous surface with well-defined pores and cavities, which play a crucial role in providing a high surface area, enhancing the material's effectiveness in adsorption processes.

Milling and other mechanical processing methods can produce fragmented fibres and irregularly shaped particles, with sizes ranging from  $49.59 \mu m$  to  $81.06 \mu m$ . The heterogeneous texture, featuring protrusions, cracks, and layered structures, offers numerous binding sites, enhancing its efficiency as a biosorbent for dye molecules [31].

SEM images of WBS biosorbent after adsorption of MG dye are shown in Fig. 3b, where significant morphological changes appeared in the biosorbent surface after MG dye adsorption. The initially rough and porous structure exhibited noticeable alterations, including the deposition of dye molecules, which partially covered the surface features. Some pores appeared less defined, suggesting the penetration and entrapment of dye within the material. Additionally, the presence of aggregated particles and smoother regions indicates possible interactions between the MG dye and functional groups on the biosorbent.

These observations confirm the successful adsorption of MG dye, likely attributed to electrostatic attraction and hydrogen bonding, involving both physical and chemical interactions [31].

The SEM images of the WBS biosorbent after MR dye adsorption, shown in Fig. 3c, reveal a highly porous and irregular surface morphology. The structure appears rough, with numerous cavities, flakes, and fibrous formations, suggesting significant textural modifications due to dye interaction. Agglomerated and layered structures indicate possible dye deposition or surface entrapment. These morphological features contribute to the enhanced adsorption capacity, likely due to the increased surface area and available binding sites. The observed structural alterations confirm successful dye adsorption and potential chemical or physical interactions between the biosorbent and MR molecules.

In Fig. 3d, the SEM images of the WBS biosorbent after the adsorption of ARS dye reveal significant morphological modifications. Figure 3d illustrates a layered and fragmented morphology, marked by prominent plate-like structures approximately 75.80 µm in size, suggesting a relatively large microstructure. The surface appears more aggregated and rougher, indicating the attachment of dye molecules onto the WBS biosorbent structure. The presence of irregular clusters and reduced porosity suggests that the dye molecules have occupied the available adsorption sites. Additionally, the slight compaction of the fibrous structure further supports the successful interaction between the biosorbent and the dye. These observations confirm the efficient adsorption of ARS onto the WBS biosorbent, likely through electrostatic interactions and hydrogen bonding.

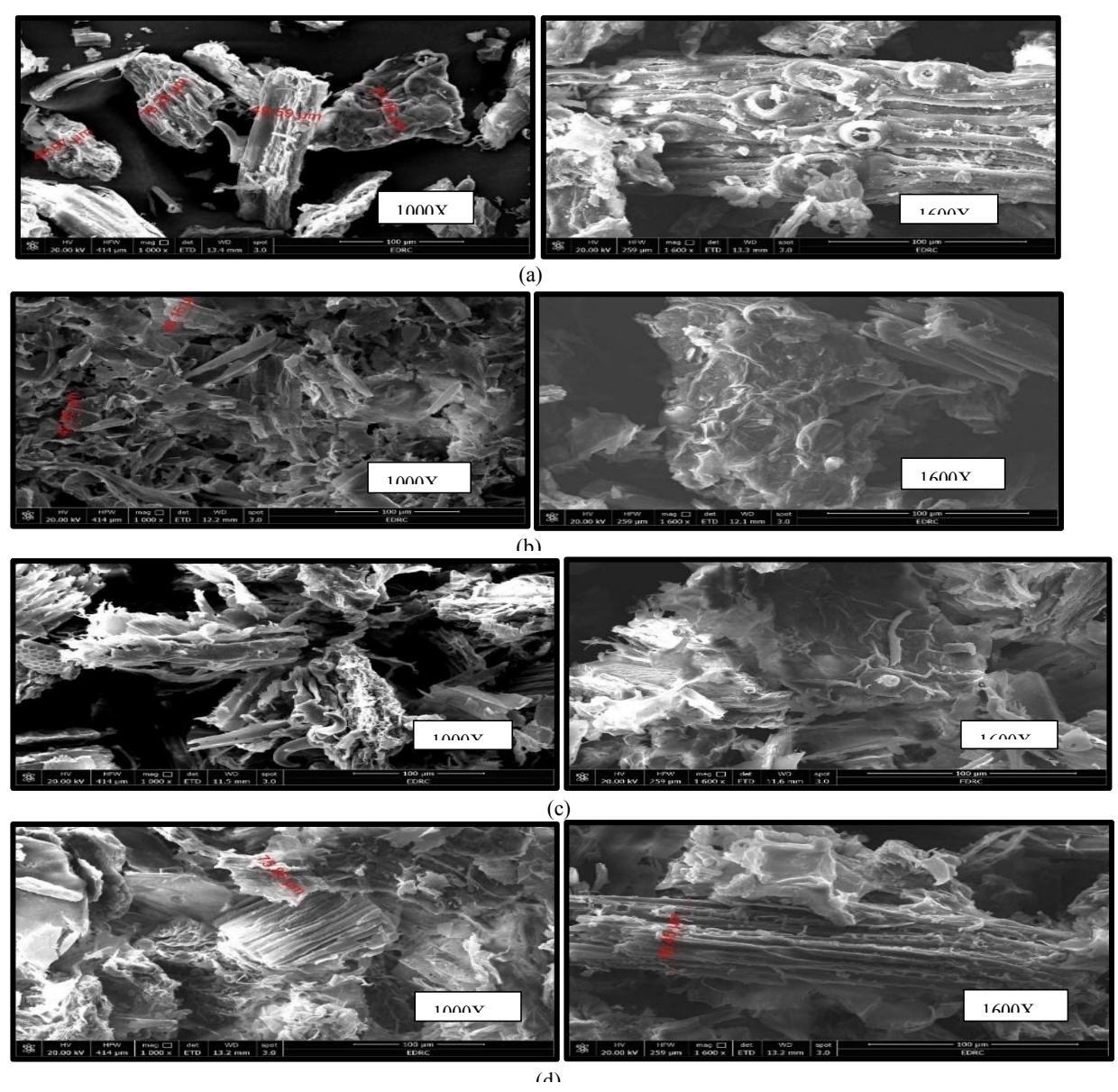


Fig. 3. SEM micrographs (a) White Bean Straw biosorbent (WBS), (b) WBS after adsorption of Malachite Green (MG), (c) WBS after adsorption of Methyl Red (MR), (d) WBS after adsorption of Alizarine Red S.

Fig. 4a represents the analysis of the biosorbent's elemental composition, conducted through Energy Dispersive X-ray Spectroscopy (EDX) before dye adsorption. The initial composition of the raw WBS biosorbent primarily consisted of 37% carbon (C), 45% oxygen (O2), and 13.9% nitrogen (N2), with minor amounts of calcium (Ca), magnesium (Mg), and silicon (Si). This elemental profile reflects the presence of both organic constituents—mainly cellulose, hemicellulose, and lignin—and mineral (ash-related) components naturally present in the biomass.

After adsorption of MG, MR, and ARS dyes, notable changes were observed in the elemental composition. In Fig. 4(b & d), the carbon content increased significantly in the MG and ARS-loaded sample, which may be attributed to the organic nature of the dye's molecules binding to the biosorbent surface. In contrast, the oxygen percentage remained nearly constant, suggesting that the adsorption process did not significantly alter the oxidation state of the surface. Chlorine (Cl) appeared in the MG-loaded sample, and sodium (Na) appeared in the ARS-loaded sample, which were absent in the raw biosorbent. This suggests that the adsorption of MG and ARS dyes involves ionic interactions, as the MG dye contains chloride counterions that may have remained attached to the surface. The presence of Cl could also indicate possible ion exchange mechanisms between the biosorbent surface and the dye molecules. The decrease in Ca and Mg content after adsorption may be due to ion exchange or surface complexation mechanisms involved in the dye removal process.

For the MR-loaded sample (Fig. 4c), a notable increase in nitrogen content was detected, indicating the successful adsorption of MR, which contains nitrogen in its molecular structure. The slight variations in Si and Ca levels suggest possible surface interactions between the dye molecules and mineral components of the biosorbent.

These results confirm the successful adsorption of both dyes onto the biosorbent material and suggest that different adsorption mechanisms may be involved, including electrostatic interactions, hydrogen bonding, and ion exchange.

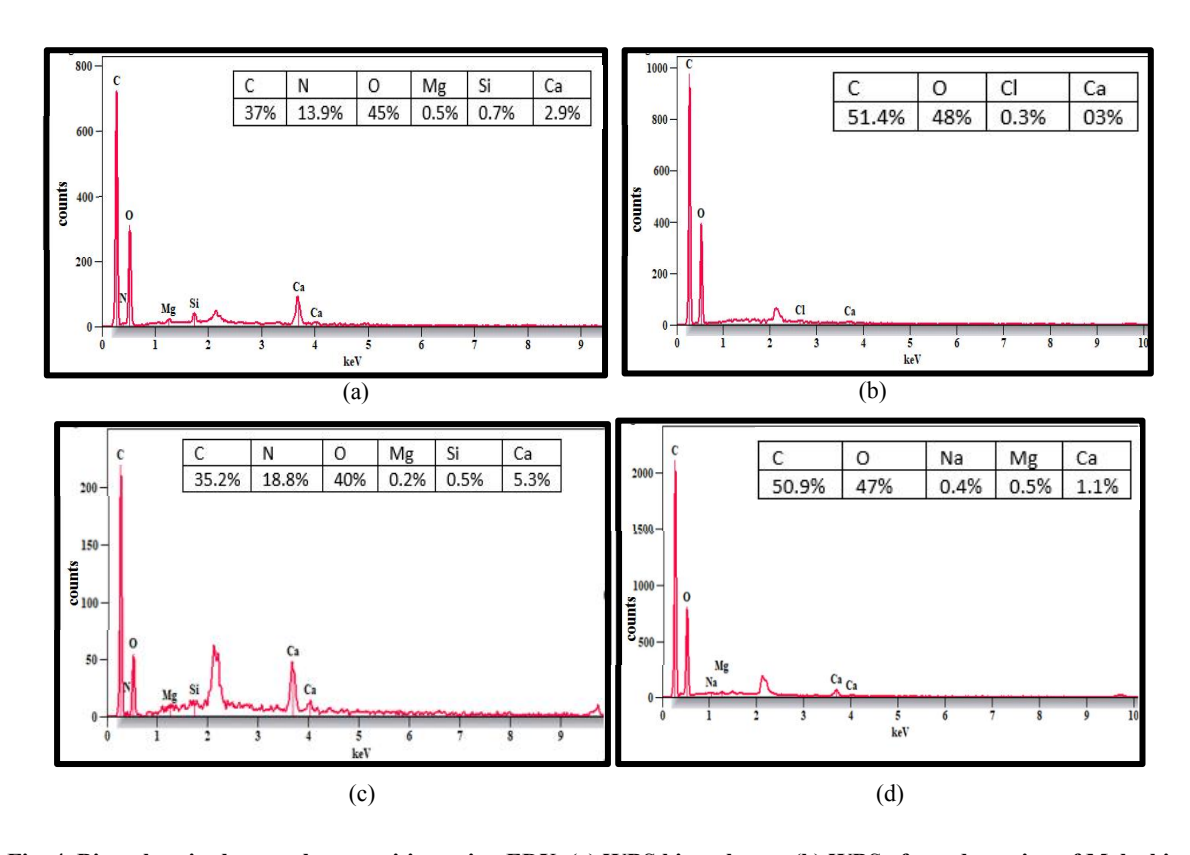


Fig. 4. Biosorbent's elemental composition using EDX, (a) WBS biosorbents, (b) WBS after adsorption of Malachite Green (MG), (c) WBS after adsorption of Methyl Red (MR), (d) WBS after adsorption of Alizarin Red S (ARS).

#### 4.1.4. Zeta potential measurements of WBS

The zeta potential is often seen as a remote effect of the surface charges of the particles. The zeta potential is positive at extremely low pH levels (about 1). It diminishes swiftly, turning negative as pH increases. The highest negative value (about -26 mV) is obtained at pH 7. The zeta potential begins to rise once more at elevated pH levels. As depicted in Fig. 5, it crosses zero at two distinct points: first at a pH of 1.7 and second at a higher pH of 10.8. The second zero point at pH 10.8 indicates that below this pH, the surface reverts to a positive charge. Within the range of pH 1.7 to 10.8, the material maintains negative and positive charges, which will be effective for adsorption of both cationic and anionic dyes.

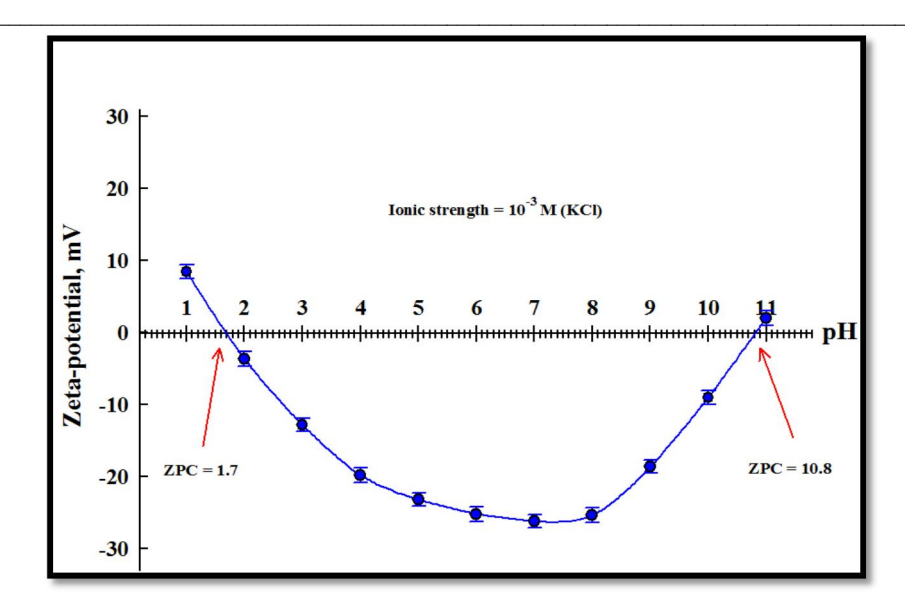


Fig. 5. Zeta potential analysis of WBS before adsorption.

#### 4.1.5. Adsorption mechanism

The adsorption of both cationic dyes (Malachite Green and Methyl Red) and the anionic dye (Alizarin Red S) onto the WBS-based biosorbent can be explained through a combination of physicochemical interactions. The FTIR spectra revealed noticeable shifts and intensity changes in key functional groups such as –OH, –COOH, –NH, and aromatic C=C bonds after dye adsorption, suggesting their active participation in the binding process. These observations indicate the occurrence of several mechanisms:

- Electrostatic interactions: between the negatively charged sites on the biosorbent surface (especially under basic conditions) and the cationic dyes.
- Hydrogen bonding: between –OH/–COOH/–NH groups on the biosorbent and polar functional groups in the dye structures.
- π-π stacking interactions: between the aromatic rings present in both the dyes and the lignocellulosic matrix of the biosorbent.

Moreover, the SEM images showed clear morphological changes and increased surface roughness after dye loading, which reflects the deposition of dye molecules on the biosorbent surface. The EDX analysis further confirmed the presence of new elements such as nitrogen and sulfur (originating from dye molecules), providing strong evidence for successful adsorption and dye—surface interaction.

Based on these findings, the proposed adsorption mechanism is illustrated in Fig.6, integrating the possible interactions responsible for dye retention on the WBS biosorbent.

#### 4.2. The impact of solution pH on WBS biosorbents

The initial investigation focused on determining the best adsorption conditions. The investigation focuses on the WBS adsorption effectiveness of Malachite Green (MG) as a cationic dye, Methyl Red (MR) as an anionic azo dye, and Alizarine Red S (ARS) as an anionic dye. pH influences the surface charge of the biosorbent, the degree of ionization of functional groups in the dye, and the biosorbent, as well as the speciation of ions like  $H^*$  and dye molecules.

Using an initial dye concentration of 25 ppm, 0.05 g of WBS particles smaller than 150 μm, and an equilibrium time of 3 hours at 25°C, the removal efficiency of MG, MR, and ARS dyes by WBS was evaluated across varying pH levels. Since ARS is greatly impacted by pH variations, as seen in Fig. 7, the pH range for ARS was 2 to 12 (wider range) compared to 2.0 to 9.0 for MG and MR dyes. The findings demonstrate that the optimum pH for MG and MR adsorption is 8, but for ARS, it is 10. The greatest removal efficiencies attained under these circumstances were 86.79% for MG, 84.78% for MR, and 41.7% for ARS. Determining the adsorbent's point of zero charge (pH\_pZC) is crucial for understanding the adsorption mechanism. Adsorption of cation dyes is more likely at pH > pH<sub>PZC</sub>, while that of anionic dyes is more likely at pH < pH<sub>PZC</sub>. When pH > 10.8 (zero-point charge), as seen in Fig. 5, the surface becomes negatively charged, which encourages the adsorption of cationic dyes. The removal of anionic dyes is facilitated by the surface becoming positively charged when pH < 1.7. The compound's mixed surface charges allow it to efficiently remove both cationic and anionic dyes in the pH range of 1.7 to 10.8. That's why MG (cationic dye) had an ideal pH of 8, and Anionic dyes' MR and ARS values were 8 and 10, respectively.

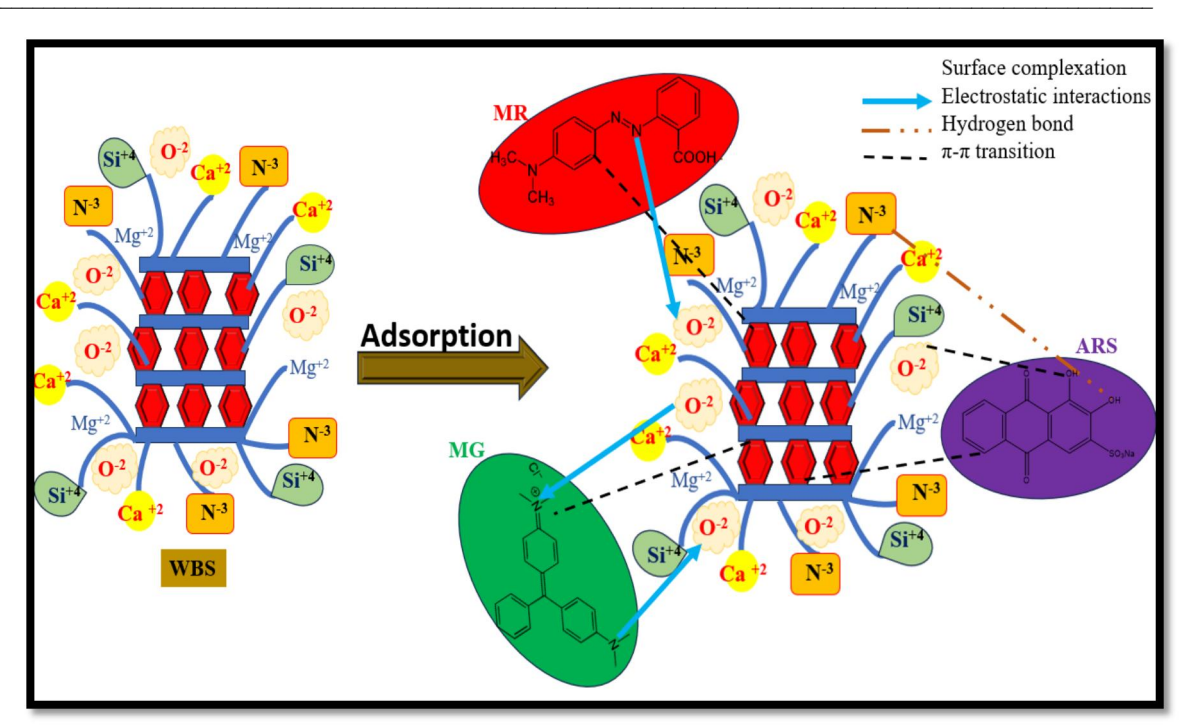


Fig. 6. Proposed adsorption mechanism of WBS with MG, MR, and ARS.

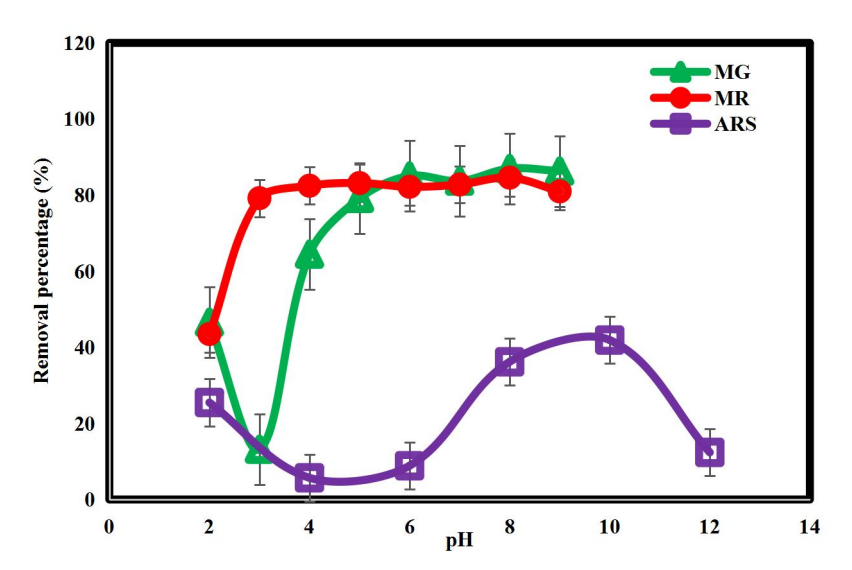


Fig. 7. The effect of the initial solution pH on the removal efficiencies of WBS biosorbent removal of MG, MR, and ARS dyes.

#### 4.3. The impact of dye concentration on adsorption

For the three dyes (MG, MR, and ARS), the effect of starting dye concentration on adsorption was investigated at initial concentrations of 5, 10, 25, 50, 100, 150, and 200 mg/L. The data presented in Fig.8 indicate that the adsorption capacity rises with the initial dye concentration across all three dyes. The noted increase can be attributed to the higher availability of dye molecules, which enhances the chances of interactions between the dye and the adsorbent surface. Consequently, more adsorption sites are filled. Once the adsorbent reaches its maximum adsorption capacity, no further increase occurs, as all active sites become saturated.

Assessing the maximum adsorption capacity and removal efficiency is important for evaluating an adsorbent's effectiveness in dye removal, offering important insights into its potential application in wastewater treatment.

After three hours, MG had the highest removal percentage observed (98.2%) at a concentration of 10 mg/L. MR achieved a maximum removal of 93.8% at 100 mg/L, whereas ARS showed a maximum removal of 61.3% at 25 mg/L.

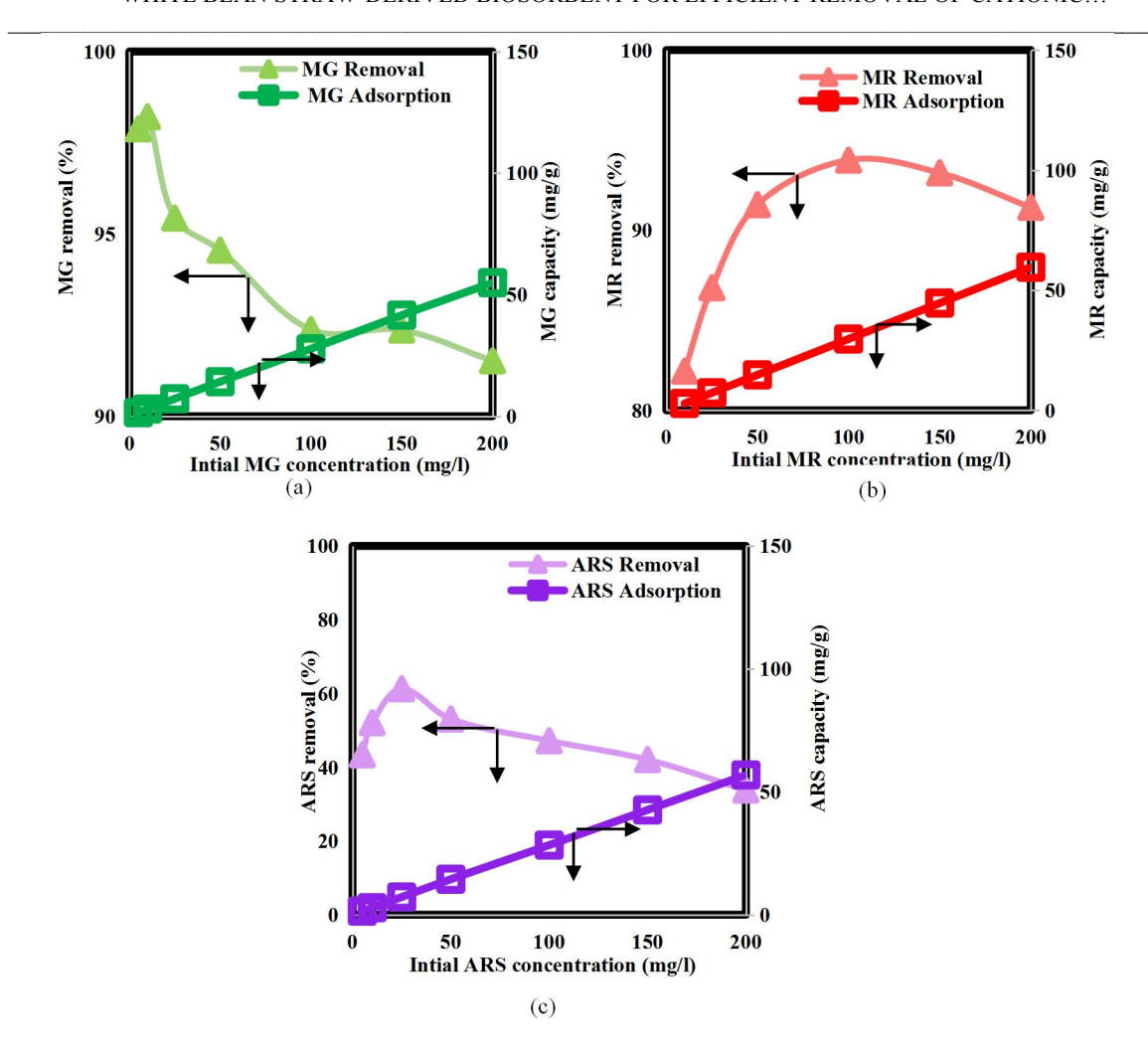


Fig. 8. The impact of starting concentration on adsorption capacity and removal percentage on (a) MG, (b) MR, and (c)ARS dyes.

## 4.4. The impact of contact time on WBS removal

Contact times varying from 0 to 180 minutes (every 15 min) were used to determine their effect on adsorption removal percentage (%). Since equilibrium had not yet been achieved and many active adsorption sites were still vacant, it was found that the adsorption removal increased with contact time. Adsorption continued until equilibrium was reached, with the adsorption sites becoming fully saturated at approximately 120 minutes.

From the results presented in Fig. 9, after 120 minutes, the maximum Removal percentage measured experimentally in this investigation were 98.2, 86.8, and 61.27 % for MG, MR, and ARS, respectively. Identifying the equilibrium point is essential, as extending contact times beyond this point leads to increased operating costs without significant gains in adsorption.

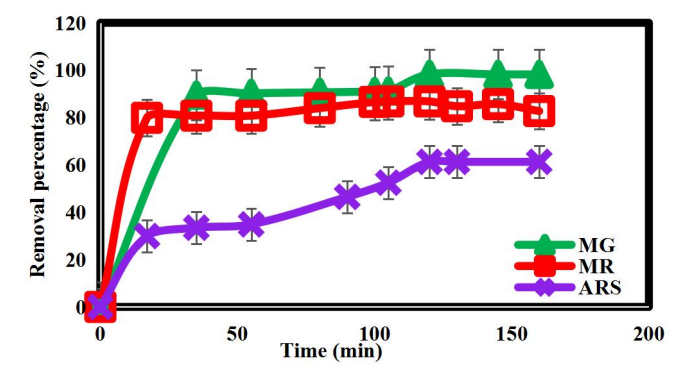


Fig. 9. The impact of contact time on MG, MR, and ARS adsorption.

4.5. The impact of WBS dosage on biosorption

The dosage of the adsorbent was a crucial element in the color removal process. Fig. 10 presents a graph illustrating the relationship between dye removal percentage and adsorbent dosage in g/L. This figure shows that when the adsorbent dosage is increased from 0.01 to 0.05 g/L, the amount of dyes removed increases. The reason for this is that there are more adsorption sites accessible. At greater dosages (0.1g/L), this benefit will end because the adsorption sites will overlap and collide, due to the higher number of unsaturated sites per mass of biosorbent. Using 0.05 g/L of WBS, the maximal experimental elimination for MG, MR, and ARS was 98.2%, 95.7%, and 61.2%, respectively.

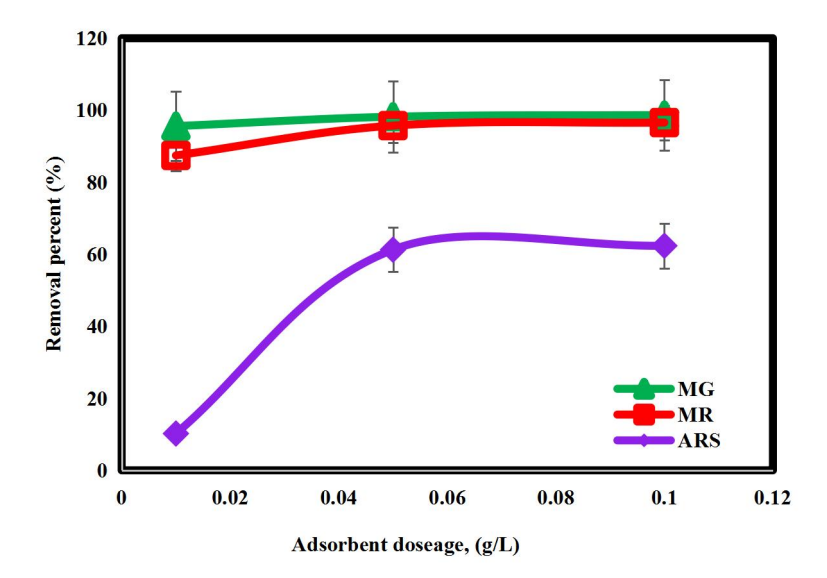


Fig. 10. Effect of WBS dose on adsorption removal percent.

4.6. The impact of particle size on removal percentage

Three particle size ranges were utilized to examine how particle size influences adsorption: greater than 300  $\mu$ m, less than 300  $\mu$ m but greater than 150  $\mu$ m, and less than 150  $\mu$ m. The results of the analysis recorded after two hours and illustrated in Fig. 11, showing that adsorption efficiency for MG and ARS is improved by decreasing particle sizes. Adsorption mostly takes place on the adsorbent's surface, where MG and ARS had removal efficiencies of 98.2% and 61.8%, respectively. The larger surface-to-volume ratio, which offers more accessible adsorption sites, is responsible for the higher adsorption efficiency at smaller particle sizes.

In contrast to MG and ARS, which showed better adsorption at smaller particle sizes, MR demonstrated the highest removal effectiveness (96.02%) at the biggest particle size (>300  $\mu$ m). This implies that for MR, adsorption might be influenced by a variety of parameters, including pore structure, diffusion mechanisms, and interactions between the dye and the adsorbent, in addition to the surface area. In comparison to bigger particles, the smaller particles may exhibit restricted diffusion or distinct binding behavior, which would result in no appreciable improvement in adsorption. The particles below 150  $\mu$ m were successful, thus, this size was adopted in all of the research.

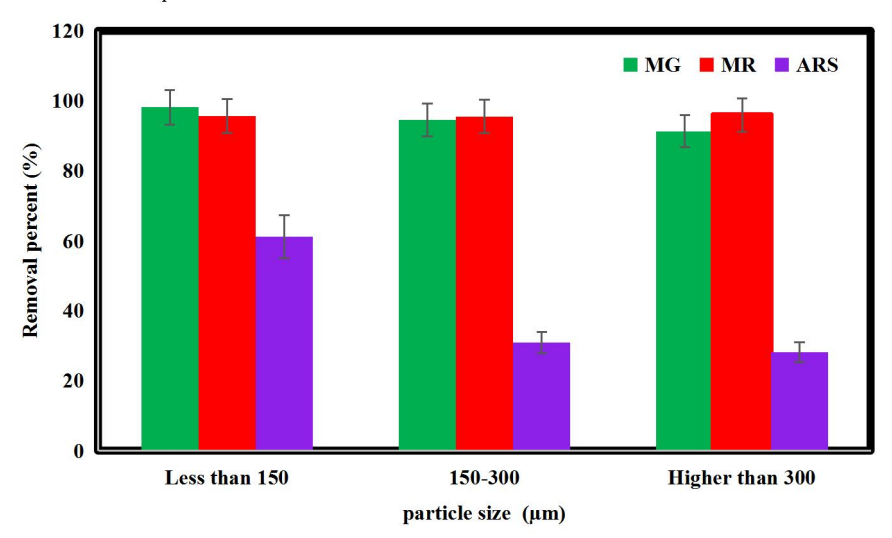


Fig. 11. Effect of particle size on removal percentage.

4.7. The impact of dye solution temperature on adsorption

The impact of temperature on biosorption was examined at 25°C, 35°C, and 45°C. As mentioned in section 4.4, for MG, MR, and ARS, the optimal dye concentrations with the highest elimination efficiency were 10 mg/L, 100 mg/L, and 25 mg/L, respectively. Since adsorption is at lower temperatures, the results shown in Fig. 12 suggest that the process is exothermic. Since the energy of the adsorbed state is less than that of the free dye molecules in the solution, this energy release takes place. The process's exothermic nature allows it to be efficiently conducted at room temperature without requiring additional heating. Moreover, operating at room temperature ensures that the size of the filtration system is not constrained by temperature, enhancing both the scalability and cost-effectiveness of the process.

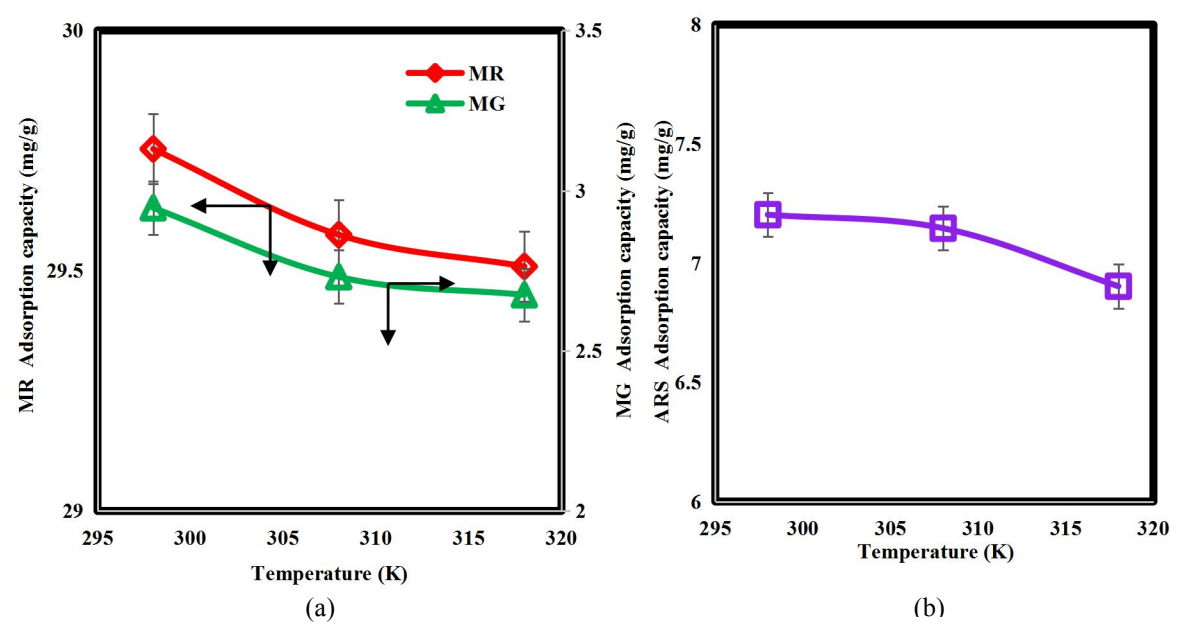


Fig. 12. Effect of solution temperature on (a) MG and MR, (b) ARS adsorption capacity.

#### 4.8. Adsorption isotherms

The equilibrium between the dye concentration in the bulk solution and the dye absorbed by the adsorbent can be theoretically described using an isotherm model [32]. The biosorbent examined in this study employed the Langmuir and the Freundlich isotherm models. The Langmuir isotherm equation is presented in Eq. 6:

$$q_c = \frac{Q_{\text{max}} K_L C_c}{1 + K_L C_c} \tag{6}$$

where  $q_e$  is the amount of adsorbate adsorbed per unit mass of adsorbent,  $C_e$  is the equilibrium solution adsorbate concentration (mg/L),  $K_L$  is the Langmuir isotherm constant, which is connected to the binding site affinity and the adsorption free energy (L/mg),  $Q_{max}$  is the maximum amount of adsorbate adsorbed at equilibrium when the adsorbent is saturated (mg/g), and Eq. 7, which is based on the Langmuir isotherm constant, can be used to get the separation factor ( $R_L$ ), i.e. the adsorption process's favorability. Adsorption can be classified as irreversible ( $R_L = 0$ ), favorable ( $R_L < 1$ ), linear ( $R_L = 1$ ), or unfavorable ( $R_L > 1$ ) [33].  $C_0$  is the starting concentration (mg/L).

$$R_L = \frac{1}{1 + K \cdot C_0} \tag{7}$$

The Langmuir isotherm model assumes a uniform surface with evenly distributed adsorption energy, a single adsorbed molecule per adsorption site, no interaction between molecules, monolayer adsorption, and the irreversibility of the process [34]. These assumptions facilitate the calculations of monolayer capacity.

For MG, MR and ARS, the separation factor (RL) was 0.2,0.6, and 0.3, respectively at a concentration of 5 mg/L for MG and ARS and 10 mg/L for MR. At 200 mg/L, the separation factor was 0.007,0.08, and 0.01 for MG, MR, and ARS, respectively. It can be concluded that the process is favorable within these ranges of concentrations for each dye as RL < 1.

However, according to the Freundlich adsorption isotherm model, which was created in 1906 [35] The adsorbent material has a heterogeneous surface with a variety of active adsorption sites. Additionally, this model can accommodate multilayer adsorption. The Freundlich model explains multilayer adsorption when physisorption is the dominating process, but it adequately captures monolayer adsorption when chemisorption is dominant. Eqs. 8 and 9 present the nonlinearized and linearized Freundlich isotherm equations, respectively:

$$q_e = K.C_e^{1/n} \tag{8}$$

$$Log \ q_e = log \ K_f + 1/n \ log \ C_e$$
 where n is the strength coefficient and  $K_f$  is the coefficient of the Freundlich isotherm model (mg/L). Temperature and

where n is the strength coefficient and  $K_f$  is the coefficient of the Freundlich isotherm model (mg/L). Temperature and adsorption parameters, such as surface heterogeneity or adsorption capacity, affect the value of 1/n [36].

When the process does not meet the criteria of the Langmuir isotherm, as in situations involving heterogeneous surfaces and multi-layering, the Freundlich model can be used [37]. For comparison, the experimental data are shown in Fig. 13 together with the two isotherm models, computed and shown in Table 3.

Table 3: The isotherms of the Langmuir and the Freundlich models' adsorption parameters.

Isotherm Model	Parameter	MG	MR	ARS
Experimental	Q <sub>max,exp</sub> (mg/g)	54.9	59.5	56.8
Langmuir	$Q_{max}(mg/g)$	31.25	20	30.12
	$K_L(L/mg)$	0.487	0.0616	0.316
	$R_{ m L}$	0.2 - 0.007	0.6 - 0.08	0.3 - 0.01
	$\mathbb{R}^2$	0.9791	0.8764	0.9553
	SSE	996.77	5544.47	1678.9
	RMSE	11.93	30.399	15.49
Freundlich	$K_f(mg/L)$	7.5	24.457	6.839
	1/n	0.6776	3.0884	0.887
	$\mathbb{R}^2$	0.9912	0.9682	0.9864
	SSE	26.17	384.52	19.87
	RMSE	1.93	8	1.69

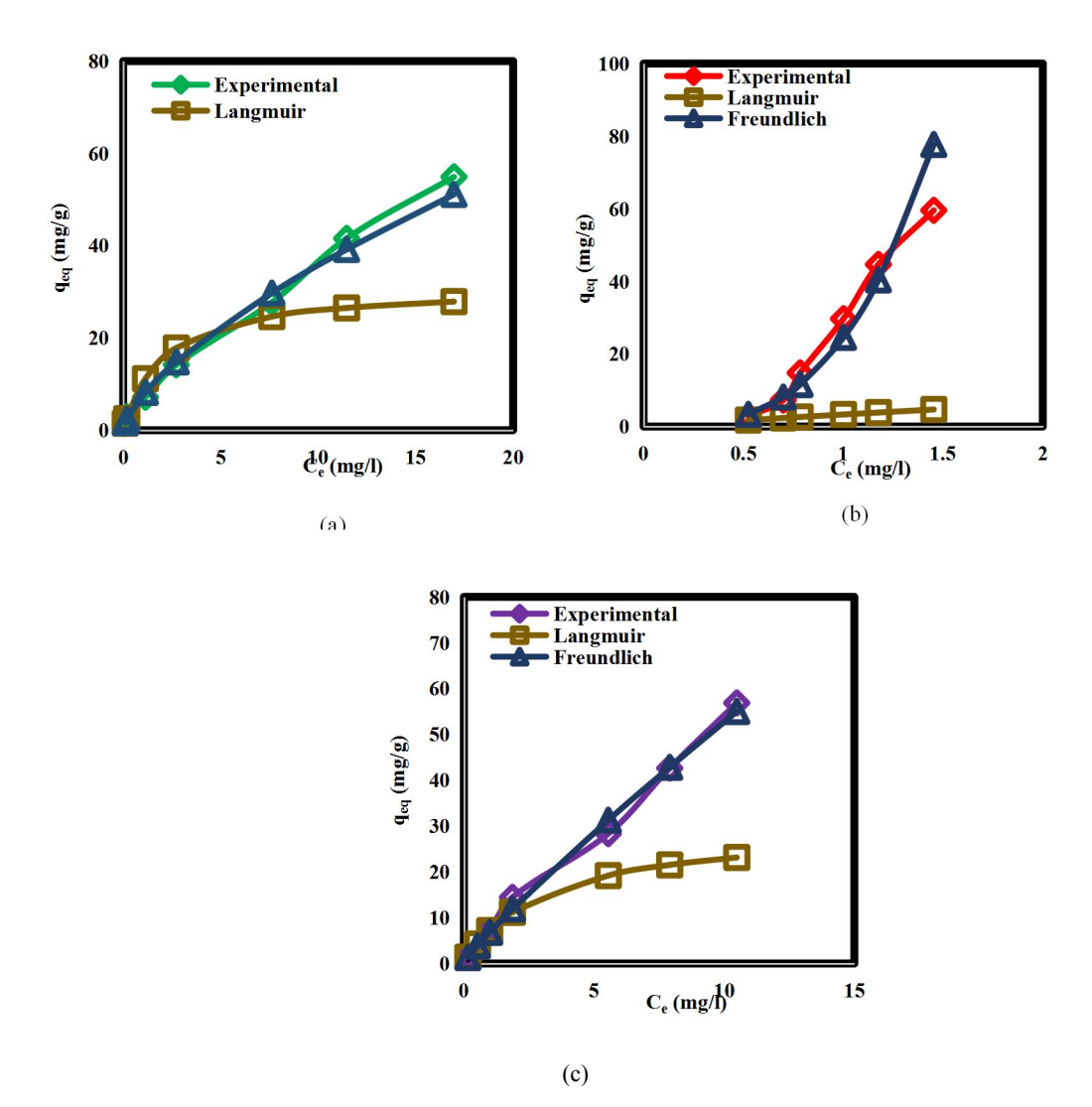


Fig. 13. Langmuir isotherm, Freundlich isotherm, and experimental isotherm for (a) MG, (b) MR, and (c) ARS.

As shown in Fig. 13, For all dyes MG, MR, and ARS, the Freundlich isotherm demonstrated a superior  $R^2$  value along with reduced SSE and RMSE values when compared to the Langmuir isotherm. So, the Freundlich isotherm was the only model that adequately represented the experimental data.

#### 4.9. Adsorption kinetics

Kinetic models are essential for evaluating functional performance, interpreting the interactions between adsorbents and pollutants, and understanding the complexities of the adsorption process. There are various kinetic models, including pseudo-first-order (PFO) [38], and pseudo-second-order (PSO) [39] which were utilized in this study.

Based on Eq. 10, the pseudo-first-order model is the most commonly used for the liquid-solid adsorption [40].

$$ln(q_c - q_t) = ln(q_c) - K_I t$$
 (10)

Where  $q_e$  represents the quantity of adsorbate present in the adsorbent at equilibrium (mg/g),  $q_t$  is the quantity of adsorbate in the adsorbent at a specific time t (mg/g),  $K_1$  is the rate constant associated with first order (min<sup>-1</sup>), and t indicates the contact time (min).

The kinetics of pseudo-second-order reactions involve adsorption occurring at two surface sites. The second-order differential equation Eq. 11 can be used to depict this process [41].

$$\frac{t}{Q_t} = \frac{1}{K_2 Q_c^2} + \frac{1}{Q_c} t \tag{11}$$

Where  $K_2$  (g/mg. min) is the adsorption rate constant for pseudo-second-order adsorption, and  $q_e$  and  $q_t$  are the amounts of adsorption dye (mg/g) at equilibrium and at time t, respectively.

The parameters of the kinetic models are calculated using Eqs. 10 & 11, and presented in Table 4 and Fig.14 alongside the experimental values for comparative analysis.  $q_{e,exp}$  represents the maximum experimental adsorption attained at 10 mg/L for MG and 25 mg/L for MR and ARS.  $q_{e(cal)}$  represents the theoretical adsorption capacity, calculated from Eqs. 11 & 12. For the three dyes, the PSO kinetic model exhibited a higher  $R^2$  value along with lower SSE and RMSE compared to the PFO kinetic model. The values of  $q_{e(cal)}$  in the pseudo-second order closely matched those of  $q_{e(exp)}$ . The PSO kinetic model is applicable for describing the process. The majority of biosorbents can be characterized by PSO kinetics.

#### 4.10.Adsorption thermodynamic parameters

Accurate calculations of the thermodynamic values: Gibbs' free energy  $\Delta G^{\circ}$ , enthalpy  $\Delta H^{\circ}$ , and entropy  $\Delta S^{\circ}$  are essential for gaining deeper insights into the characteristics of the contaminant adsorption technique, including its thermodynamic behavior (whether endothermic or exothermic), spontaneity, and overall feasibility. The variation of  $\Delta G^{\circ}$ ,  $\Delta H^{\circ}$ , and  $\Delta S^{\circ}$  can be calculated at different temperatures using Eq. 12&14

$$\Delta G = -RT \ln \left(K_{c}\right) \tag{12}$$

Where  $\Delta G$  represents the change in Gibbs free energy (J/mol), R is the universal gas constant (8.314 J/mol.K), T is the absolute temperature (K), and Kc is the thermodynamic equilibrium constant, which can be determined using Eq.13:

$$K_c = \frac{C_{Ads,e}}{C_e} \tag{13}$$

Where C<sub>Ads,e</sub> refers to the concentration of dye adsorbed by the adsorbent at equilibrium (mg/L).

Gibbs free energy can also be expressed in Eq.14

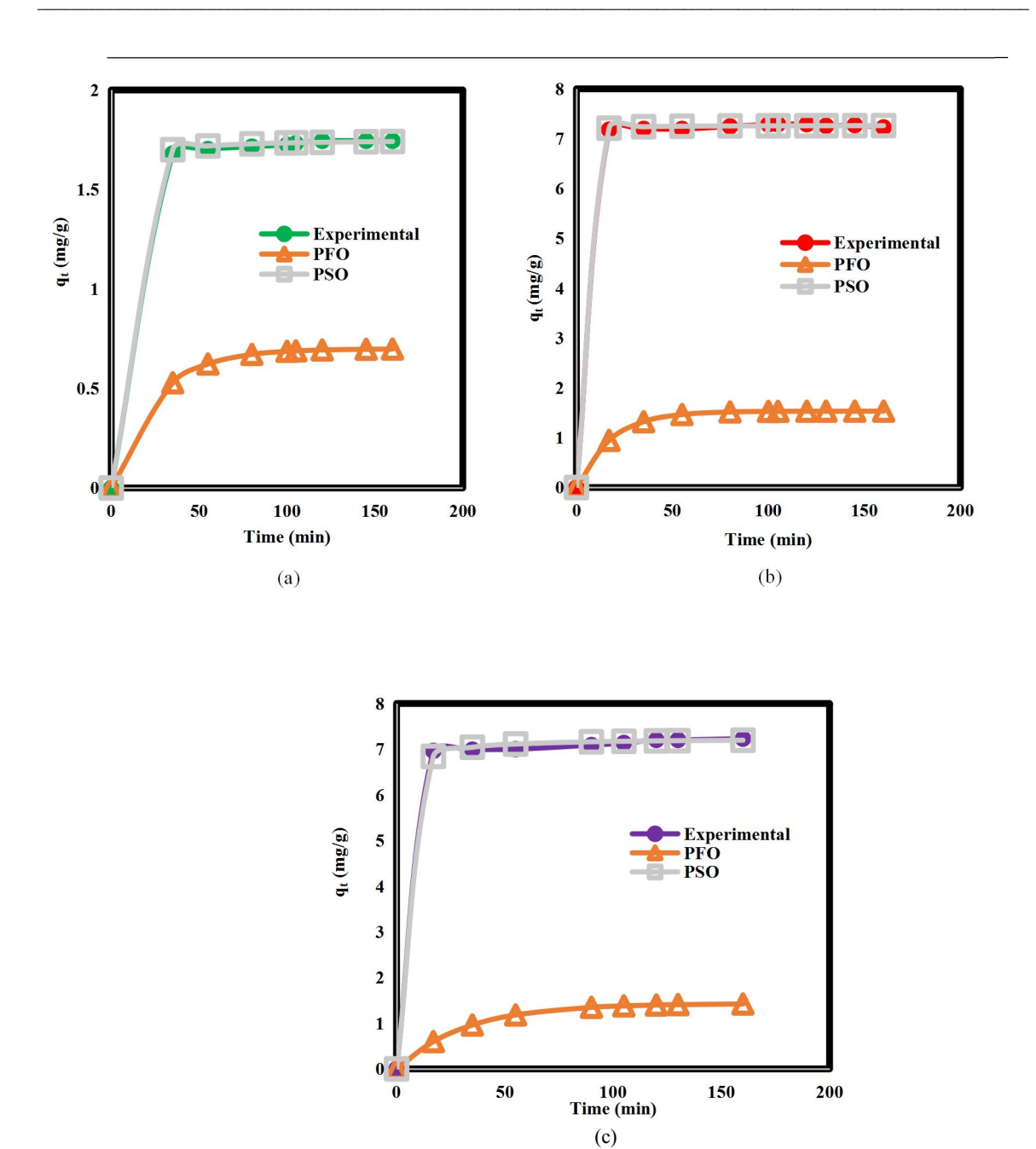
$$\Delta G = \Delta H - T \Delta S \tag{14}$$

Where  $\Delta H$  is the enthalpy change (J/mol),  $\Delta S$  is the entropy change (J/mol K), and T is the absolute temperature (K). The variations in entropy and enthalpy can be derived from the slope and intercept of the graph plotting Gibbs free energy against temperature, as illustrated in Fig. 15. When molecules migrate from a higher-entropy state (solution) to a more ordered state (on the solid surface), entropy is negative [42]. chemisorption is indicated by values of -217.36 J/mol.K. for MG, while physical adsorption is indicated by values of -52.301 J/mol.K. and -71.348 J/mol.K. for MR and ARS.

Table 5 shows all the thermodynamic data. The enthalpy is negative, indicating that the adsorption process is exothermic. The process is thermodynamically spontaneous, as the Gibbs free energy value is negative.

**Table 4: Kinetic model parameters.** 

, rrincere mouer parame	***				
Model	Parameter	MG	MR	ARS	
Experimental	q <sub>e,exp</sub> (mg/g)	1.74	7.29	7.202	
Pseudo-first-order	$q_{e(cal)}(mg/g)$	0.698	1.53	1.43	
	$K_{l}(\min^{-1})$	0.0403	0.0564	0.0318	
	$\mathbb{R}^2$	0.8465	0.7631	0.631	
	SSE	9.05	271.37	277.82	
	RMSE	1	4.967	5.56	
Pseudo-second-order	$q_{e(cal)}(mg/g)$	1.753	7.27	7.24	
	$\widehat{K}_2$ (g mg <sup>-1</sup> min <sup>-1</sup> )	0.522	1.007	0.139	
	$\mathbb{R}^2$	0.9999	0.9999	0.9998	
	SSE	0.00098	0.0089	0.038	
	RMSE	0.0105	0.028	0.065	



 $Fig. 14. \ The \ pseudo-first-order \ model \ and \ pseudo-second-order \ model \ plotted \ with \ experimental \ results \ for \ (a) \ MG, \ (b) \ MR, \ and \ (c) \ ARS \ dyes.$ 

Table 5: The thermodynamic variables of MG, MR, and ARS.

Dye	Temperature (K)	Kc	ΔG(J/mol)	ΔH(kJ/mol)	ΔS (J/mol K)
Malaabita assass	298	54.73	-9.916		
Malachite green	308	10.15	-5.934	-74.087	-217.36
(MG)	318	8.22	-5.569		
Madhad and	298	120.64	-11.875		
Methyl red	308	69.55	-10.863	-27.297	-52.301
(MR)	318	60.08	-10.829		
Alizarin Red S (ARS)	298	24.23	-7.898		
	308	20.19	-7.695	-29.330	-71.348
	318	11.56	-6.471		

Egypt. J. Chem. 69, No. 2 (2026)

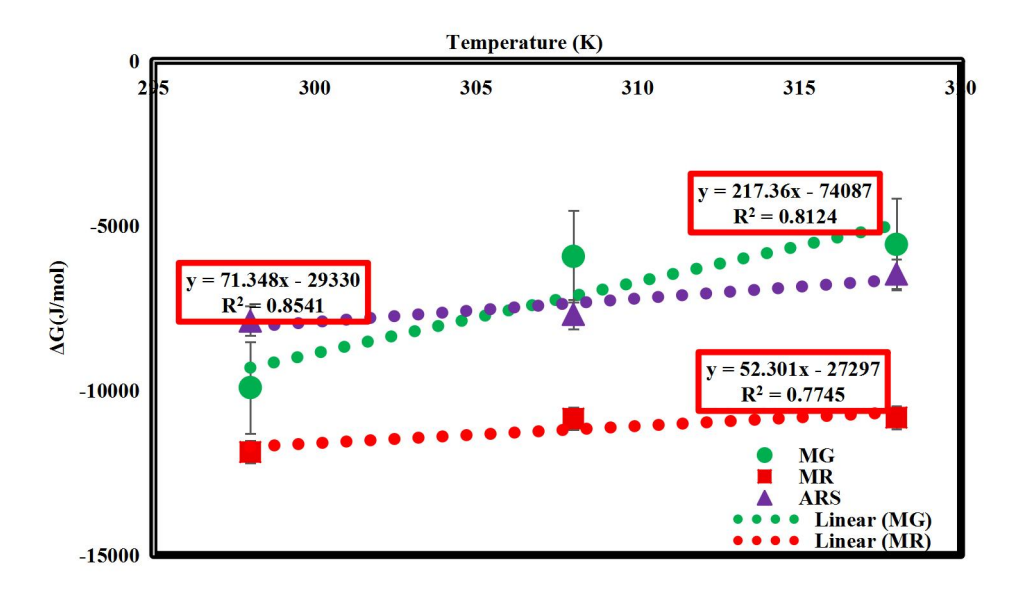


Fig.15. Gibb's free energy changes with temperature for MG, MR, and ARS.

#### 4.11. Selectivity for a mixture of the three dyes.

Selectivity refers to the favored adsorption of one dye over others, influenced by differences in molecular structure, functional group interactions, and electrostatic charge affinities. This work uses experimental comparison to assess the preferential adsorption of cationic Malachite Green, anionic Alizarin Red S, and anionic Methyl Red on White Bean Straw.

As mentioned in section 4.1.4, WBS zeta potential tests showed two zero potential points of 1.7 and 10.8, making it an effective adsorbent for both cationic and anionic dyes.

The molecular sizes of these dyes play a significant role in their adsorption behavior; larger molecules, such as MG and ARS, can experience steric hindrance within micropores, whereas smaller molecules, like MR, can penetrate and diffuse more easily into these microscopic pores. Table 6 displays the other structural and chemical distinctions.

Table 6: Structural and chemical differences between MG, MR and ARS.

Property	Malachite Green (MG)	Methyl Red (MR)	Alizarin Red S (ARS)
Chemical Structure	Triphenylmethane dye	Azo dye (-N=N-)	Anthraquinone dye
Molecular Size (Å)	~14.2	~10.5	~11.5
Charge at Neutral pH	Cationic (+)	Anionic (-)	Anionic (-)
Solubility in Water (mg/L)	High	Moderate	High
Functional Groups	-C-NH- (amine)	-COOH, -N=N-	Contains hydroxyl (-OH) &carboxyl (-COOH) groups

Experimentally, three samples with different pH and concentrations were prepared as follows:

Sample 1: 25 mg/L of each dye, all at pH 8.

**Sample 2**: optimum concentration for each dye as reached experimentally, as mentioned in section 3.2: 10 ppm for MG, 100 ppm for MR, and 25 ppm for ARS, all at pH 8.

Sample 3: optimum concentration of each dye, all at their natural pH (8.8 for MG, 7.4 for MR, and 9 for ARS).

 $0.05\,\mathrm{g}$  of less than  $150\,\mu\mathrm{m}$  WBS was added to 5 mL of each sample with the conditions mentioned above. The solution was agitated at  $120\,\mathrm{rpm}$  for 2 h. Then, the solution was filtered and analyzed using UV–Vis to find the selective dye based on the calculated  $q_e$ . The absorbance data from the spectrophotometer for the three samples before and after adsorption are shown in Fig. 16.

The wavelength for MG, MR, and ARS was around 617 nm, 521 nm, and 433 nm, respectively, as the peaks for the three dyes are visible in Fig. 15, particularly for sample 1. Each dye's absorbance was measured at the same wavelength both before and after adsorption, and the concentrations were then computed. To compare the three samples, adsorption capacities can be calculated using Eq.1, and the results are shown in Table 7.

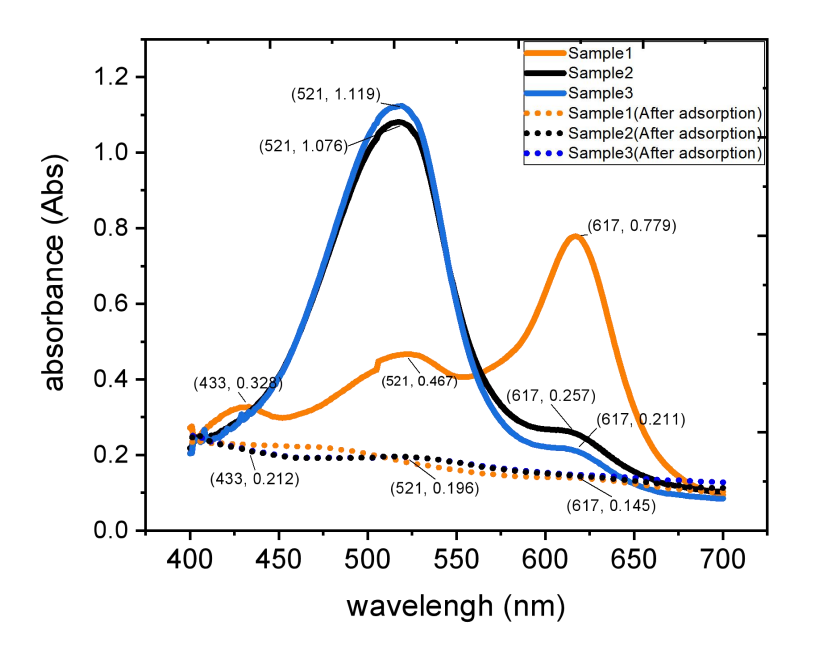


Fig. 16. The spectrum of the three samples before and after adsorption.

Table 7: Adsorption capacities for MG, MR & ARS dyes.

Dye/sample condition	q <sub>e</sub> [Sample 1] (25 ppm, pH8)	q <sub>e</sub> [Sample 2] (opt. conc, pH8)	q <sub>e</sub> [Sample 3] (opt. conc, Nat.pH)-
Malachite Green (MG)	7.157	2.631	2.633
Methyl Red (MR)	7.171	29.645	29.647
Alizarin Red S (ARS)	6.887	6.927	6.933

From Table 7, we concluded that WBS is selective to MR over the two other dyes, as MR has the highest qe.

## 4.12.Comparative Evaluation of WBS and Other Biosorbents in Terms of Adsorption Performance and Sustainability

Table 8 presents a comparative overview of the adsorption parameters for MG, MR, and ARS dyes using various adsorbents. White bean straw (WBS) exhibited high adsorption efficiency for MG and MR dyes, and moderate to high performance for ARS dye. Compared to other biosorbents listed in the table, WBS offers a balanced combination of good removal capacity, ease of preparation, and minimal processing requirements. Unlike some chemically modified or nano-based adsorbents that require complex synthesis and higher costs, WBS is locally available, requires no activation steps, and can be used in its raw or simply treated form. These advantages reduce operational costs and material consumption, making WBS a cost-effective and sustainable biosorbent for practical wastewater treatment applications.

Table 8: Comparison between MG, MR, and ARS dyes adsorption using various adsorbents.

Adsorbent	dye	pН	Time (min)	Removal%/ Capacity (mg/g)	Ref.
3-aminopropyltriethoxysilane	ARS	< 6	20	18.2 mg/g	[43]
Polypyrene-coated Fe <sub>3</sub> O <sub>4</sub> nanoparticles	ARS	4-5.4	60	116.3 mg/g	[44]
Chitosan	ARS	2	10	42.48 mg/g	[45]
Sulfuric Acid-	ARS	3	30	90.53%	[46]
Modified Avocado Seeds					
Phenyl/amine end-capped tetraaniline	ARS	5–6	30	236 mg/g	[47]
(TANI)					
Lantana camara	ARS	2	80	90 %	[48]
sheep wool	ARS	2	90	93.2%	[49]
Chicken feathers	ARS	-	-	157 mg/g	[50]

biochar-based nanocomposite	ARS	5	60	250 mg/g	[51]
Reduced graphene oxide	MG	8	120	96.3%	[52]
Sodium carboxymethyl cellulose	MG	10	120	3.26 mg/g 96.92 %	[53]
Rice Husk	MG	10	-	8.688 mg/g	[54]
palm leaves powder	MG	-	60	95 %	[55]
Oil Palm Empty Fruit Bunch	MG	-	420	94.5%	[56]
chlorella-based biomass	MG	7	60	18.7 mg/g	[57]
zinc oxide nanoparticle loaded on					
activated carbon	MG	7	15	95%	[58]
Sphagnum peat moss (SPM)	MG	6.5	60	121.95 mg/g	[59]
Activated Potassium Hydroxide Clove Leaf A growaste	MG	6	120	31.6 mg/g	[60]
NaAlg-g-CHIT/nZVI	MR	3	60	68%	[61]
White Potato Peel Powder	MR	2	80	30.48 mg/g	[62]
Activated Carbon	MR	4	100	82.81%	[63]
Banana Trunk Fibers	MR	3	80	96 %	[64]
WBS- adsorbent	ARS	10	120	61.3%	
WBS- adsorbent	MG	8	120	98.2%	₹ <sup>E</sup>
WBS- adsorbent	MR	8	120	93.8%	Current work

#### 5. Conclusion

In this research, MG, MR and ARS were extracted from a dye mixture using WBS. The material was characterized by FTIR, XRD, and SEM–EDX. The surface was identified as mainly comprising carbon and oxygen, exhibiting roughness and heterogeneity. Analysis of the primary biomass components confirmed the presence of hydroxyl, carboxyl, and aromatic functional groups, all of which contribute effectively to adsorption. The impact of contact time, adsorbent dose, starting dye concentration, particle size, pH, and temperature were examined for WBS. A small particle size of less than 150 µm, a dosage of 0.05 g/L, and an agitation of 120 rpm for 2 hours at a lower temperature of 25°C were all recommended to optimize the adsorption process for all dyes.

The pseudo-second-order model effectively explained the observed adsorption kinetics of WBS, while the Freundlich isotherm model provided the most fitted model of the adsorption isotherms for MG, MR, and ARS. The feasibility and spontaneity of the adsorption process were assessed using calculated thermodynamic parameters like entropy, enthalpy, and Gibbs' free energy. The biosorption process was exothermic and spontaneous at low temperatures, according to the thermodynamic analysis. The removal efficiency reached approximately 98.2%, 95.7% and 61.2% for MG, MR, and ARS respectively. This study highlighted the effectiveness of WBS as a biosorbent, demonstrating its enhanced efficiency in removing both cationic and anionic dyes. Thus, WBS is a novel and exciting option for treating wastewater and will be particularly helpful in recently industrialized nations that are facing severe water contamination and need a prompt, affordable, and efficient remedy. WBS regeneration, physical or chemical treatment to improve its adsorption to other pollutants, and economic analysis are possible for future research topics.

#### 6. Conflicts of interest

There are no conflicts to declare.

#### 7. References

- [1] S. Dave, J. Das, B. Varshney, and V. P. Sharma, "Dyes and Pigments: Interventions and How Safe and Sustainable Are Colors of Life!!!," *Environmental Science and Engineering*, pp. 1–20, 2022, doi: 10.1007/978-3-031-08991-6 1/TABLES/2.
- [2] H. Ben Slama *et al.*, "Diversity of Synthetic Dyes from Textile Industries, Discharge Impacts and Treatment Methods," *Applied Sciences 2021, Vol. 11, Page 6255*, vol. 11, no. 14, p. 6255, Jul. 2021, doi: 10.3390/APP11146255.
- [3] C. O. Okoye *et al.*, "Toxic Chemicals and Persistent Organic Pollutants Associated with Micro-and Nanoplastics Pollution," *Chemical Engineering Journal Advances*, vol. 11, p. 100310, Aug. 2022, doi: 10.1016/J.CEJA.2022.100310.
- [4] H. Alzain, V. Kalimugogo, and K. Hussein, "A Review of Environmental Impact of Azo Dyes," *International Journal of Research and Review*, vol. 10, no. 6, pp. 64–689, Jun. 2023, doi: 10.52403/ijrr.20230682.
- [5] U. Kumari, "Textile Dyes and Their Impact on the Natural Environment," 2024, pp. 17–30. doi: 10.1007/978-981-97-5341-3 2.
- [6] A. M. Elgarahy, K. Z. Elwakeel, S. H. Mohammad, and G. A. Elshoubaky, "A critical review of biosorption of dyes, heavy metals and metalloids from wastewater as an efficient and green process," *Clean Eng Technol*, vol. 4, p. 100209, Oct. 2021, doi: 10.1016/j.clet.2021.100209.
- [7] T. A. Aragaw, "Recovery of iron hydroxides from electro-coagulated sludge for adsorption removals of dye wastewater: Adsorption capacity and adsorbent characteristics," *Surfaces and Interfaces*, vol. 18, Mar. 2020, doi: 10.1016/J.SURFIN.2020.100439.

- [8] J. C. Coura, D. Profeti, and L. P. R. Profeti, "Eco-friendly chitosan/quartzite composite as adsorbent for dye removal," *Mater Chem Phys*, vol. 256, p. 123711, Dec. 2020, doi: 10.1016/j.matchemphys.2020.123711.
- [9] Y. Bentahar, K. Draoui, C. Hurel, O. Ajouyed, S. Khairoun, and N. Marmier, "Physico-chemical characterization and valorization of swelling and non-swelling Moroccan clays in basic dye removal from aqueous solutions," *Journal of African Earth Sciences*, vol. 154, pp. 80–88, Jun. 2019, doi: 10.1016/J.JAFREARSCI.2019.03.017.
- [10] T. Alp Arici, "Highly reusable plant-based biosorbent for the selective methylene blue biosorption from dye mixture in aqueous media," *International Journal of Environmental Science and Technology*, vol. 19, no. 3, pp. 1849–1860, Mar. 2022, doi: 10.1007/S13762-021-03238-W.
- [11] D. L. Postai, C. A. Demarchi, F. Zanatta, D. C. C. Melo, and C. A. Rodrigues, "Adsorption of rhodamine B and methylene blue dyes using waste of seeds of Aleurites Moluccana, a low cost adsorbent," *Alexandria Engineering Journal*, vol. 55, no. 2, pp. 1713–1723, Jun. 2016, doi: 10.1016/j.aej.2016.03.017.
- [12] U. Maheshwari, R. V. Thakur, D. Deshpande, and S. Ghodke, "Efficiency evaluation of orange and banana peels for dye removal from synthetic industrial effluent," *Mater Today Proc*, vol. 76, pp. 170–176, 2023, doi: 10.1016/j.matpr.2022.11.023.
- [13] A. A. Hambisa, M. B. Regasa, H. G. Ejigu, and C. B. Senbeto, "Adsorption studies of methyl orange dye removal from aqueous solution using Anchote peel-based agricultural waste adsorbent," *Appl Water Sci*, vol. 13, no. 1, pp. 1–11, Jan. 2023, doi: 10.1007/S13201-022-01832-Y/TABLES/4.
- [14] N. A. Rosli, M. A. Ahmad, and T. U. Noh, "Unleashing the potential of pineapple peel-based activated carbon: Response surface methodology optimization and regeneration for methylene blue and methyl red dyes adsorption," *Inorg Chem Commun*, vol. 155, p. 111041, Sep. 2023, doi: 10.1016/j.inoche.2023.111041.
- [15] P. R. Nimbalkar, M. A. Khedkar, P. V. Chavan, and S. B. Bankar, "Biobutanol production using pea pod waste as substrate: Impact of drying on saccharification and fermentation," *Renew Energy*, vol. 117, pp. 520–529, Mar. 2018, doi: 10.1016/j.renene.2017.10.079.
- [16] Y. Gao, H. Xia, A. P. Sulaeman, E. M. de Melo, T. I. J. Dugmore, and A. S. Matharu, "Defibrillated Celluloses via Dual Twin-Screw Extrusion and Microwave Hydrothermal Treatment of Spent Pea Biomass," *ACS Sustain Chem Eng*, vol. 7, no. 13, pp. 11861–11871, Jul. 2019, doi: 10.1021/acssuschemeng.9b02440.
- [17] V. S. Munagapati, V. Yarramuthi, Y. Kim, K. M. Lee, and D.-S. Kim, "Removal of anionic dyes (Reactive Black 5 and Congo Red) from aqueous solutions using Banana Peel Powder as an adsorbent," *Ecotoxicol Environ Saf*, vol. 148, pp. 601–607, Feb. 2018, doi: 10.1016/j.ecoenv.2017.10.075.
- [18] S. Meftah *et al.*, "The main types of derivatives of plant matter and agricultural waste used as bio-adsorbents for the removal of heavy metals and dyes: a review," *Egypt J Chem*, vol. 67, no. 9, pp. 185–207, Sep. 2024, doi: 10.21608/EJCHEM.2024.251450.8944.
- [19] M. A. Rania, E. H. Gomaa, A. G. Emam, and A. A. Elsisi, "Valorization of using agro-food waste as environmentally friendly adsorbents for toxic dye removal from their aqueous contaminated water," *Egypt J Chem*, vol. 66, no. 13, pp. 893–905, Dec. 2023, doi: 10.21608/EJCHEM.2023.192762.7582.
- [20] H. M. El Refay, A. Goma, N. Badawy, and F. Al Zahra Ghanem, "Agricultural By-Products as Green Chemistry in Elimination of Reactive Red 43 From Aqueous Media- Adsorption Properties, Kinetics and Thermodynamics Study," *Egypt J Chem*, vol. 65, no. 8, pp. 97–108, Aug. 2022, doi: 10.21608/EJCHEM.2022.102614.4757.
- [21] F. Nwosu, F. Adekola, & A. S.-P. J. of A., and undefined 2017, "Adsorption of 4-Nitrophenol (PNP) Using Pilli Nut Shell Active Carbon," *pjaec.pkFO Nwosu, FA Adekola, AO SalamiPakistan Journal of Analytical & Environmental Chemistry, 2017-pjaec.pk*, vol. 18, no. 1, pp. 69–83, Jun. 2017, doi: 10.21743/pjaec/2017.06.07.
- [22] H. Koyuncu and A. R. Kul, "Removal of methylene blue dye from aqueous solution by nonliving lichen (Pseudevernia furfuracea (L.) Zopf.), as a novel biosorbent," *Appl Water Sci*, vol. 10, no. 2, pp. 1–14, Feb. 2020, doi: 10.1007/S13201-020-1156-9/TABLES/5.
- [23] M. Sani, A. A.-C. R. and Letters, and undefined 2023, "Alizarin Red S Dye Removal from Synthetic Effluent Solution Using Untreated Typha Grass Adsorbent," *chemrevlett.com*, vol. 6, pp. 340–349, 2023, doi: 10.22034/CRL.2023.387634.1206.
- [24] M. Siminghad, S. Sheshmani, and A. S. Shahvelayati, "Application, optimisation and kinetic studies of SnO microsquare in photoinduced decolourisation of Acid Orange 7 and Acid Orange 10 under visible light irradiation," *Int J Environ Anal Chem*, vol. 101, no. 4, pp. 473–481, 2021, doi: 10.1080/03067319.2019.1668931.
- [25] H. D. Bouras *et al.*, "Biosorption characteristics of methylene blue dye by two fungal biomasses," *International Journal of Environmental Studies*, vol. 78, no. 3, pp. 365–381, May 2021, doi: 10.1080/00207233.2020.1745573.
- [26] T. Tkachenko, V. Yevdokymenko, D. Kamenskyh, Y. Sheludko, V. Povazhnyi, and V. Kashkovskyi, "Physicochemical properties of biogenic SiO2 nanoparticles obtained from agriculture residue," *Springer*, vol. 10, no. 12, pp. 4617–4623, Dec. 2020, doi: 10.1007/S13204-020-01383-1.
- [27] S. Banoth, V. S. Babu, G. Raghavendra, K. Rakesh, and S. Ojha, "Sustainable thermochemical extraction of amorphous silica from biowaste," *Springer*, vol. 14, no. 10, pp. 5289–5296, Jul. 2022, doi: 10.1007/S12633-021-01293-Z.
- [28] P. Kumar, S. B.-B. for E. Remediation, and undefined 2025, "Bio-adsorbents from biomass for environmental remediation," *Elsevier*, Accessed: Jul. 29, 2025. [Online]. Available: https://www.sciencedirect.com/science/article/pii/B978044333014800003X
- [29] E. Lima, M. Naushad, G. dos Reis, ... G. D.-...-derived materials for, and undefined 2022, "Production of carbon-based adsorbents from lignocellulosic biomass," *Elsevier*, Accessed: Jul. 29, 2025. [Online]. Available: https://www.sciencedirect.com/science/article/pii/B978032391914200012X

- [30] O. Painter *et al.*, "Preparation and Study the Structural Properties for Compound Tl0.9Hg0.1Sr2Ca2Cu3O8+δ Using the Modified Scherer Equation," *IOP Conf Ser Mater Sci Eng*, vol. 1258, no. 1, p. 012008, Oct. 2022, doi: 10.1088/1757-899X/1258/1/012008.
- [31] M. Hosny *et al.*, "Facile Synthesis of Gold Nanoparticles for Anticancer, Antioxidant Applications, and Photocatalytic Degradation of Toxic Organic Pollutants," *ACS Omega*, vol. 7, no. 3, pp. 3121–3133, Jan. 2022, doi: 10.1021/ACSOMEGA.1C06714.
- [32] A. O. Dada, F. A. Adekola, E. O. Odebunmi, A. S. Ogunlaja, and O. S. Bello, "Two-three parameters isotherm modeling, kinetics with statistical validity, desorption and thermodynamic studies of adsorption of Cu(II) ions onto zerovalent iron nanoparticles," *Scientific Reports 2021 11:1*, vol. 11, no. 1, pp. 1–15, Aug. 2021, doi: 10.1038/s41598-021-95090-8.
- [33] K. R. Hall, L. C. Eagleton, A. Acrivos, and T. Vermeulen, "Pore- and solid-diffusion kinetics in fixed-bed adsorption under constant-pattern conditions," *Industrial and Engineering Chemistry Fundamentals*, vol. 5, no. 2, pp. 212–223, May 1966, doi: 10.1021/I160018A011/ASSET/I160018A011.FP.PNG V03.
- [34] T. C. A. Siqueira *et al.*, "Sugarcane Bagasse as an Efficient Biosorbent for Methylene Blue Removal: Kinetics, Isotherms and Thermodynamics," *International Journal of Environmental Research and Public Health 2020, Vol. 17, Page 526*, vol. 17, no. 2, p. 526, Jan. 2020, doi: 10.3390/IJERPH17020526.
- [35] V. O. Shikuku and T. Mishra, "Adsorption isotherm modeling for methylene blue removal onto magnetic kaolinite clay: a comparison of two-parameter isotherms," *Appl Water Sci*, vol. 11, no. 6, pp. 1–9, Jun. 2021, doi: 10.1007/S13201-021-01440-2/TABLES/4.
- [36] M. Wasilewska, A. W. Marczewski, A. Deryło-Marczewska, and D. Sternik, "Nitrophenols removal from aqueous solutions by activated carbon temperature effect of adsorption kinetics and equilibrium," *J Environ Chem Eng*, vol. 9, no. 4, p. 105459, Aug. 2021, doi: 10.1016/j.jece.2021.105459.
- [37] L. Bo, F. Gao, Shuangbao, Y. Bian, Z. Liu, and Y. Dai, "A novel adsorbent Auricularia Auricular for the removal of methylene blue from aqueous solution: Isotherm and kinetics studies," *Environ Technol Innov*, vol. 23, p. 101576, Aug. 2021, doi: 10.1016/J.ETI.2021.101576.
- [38] R. Ezzati, S. Ezzati, and M. Azizi, "Exact solution of the Langmuir rate equation: New Insights into pseudo-first-order and pseudo-second-order kinetics models for adsorption," *Vacuum*, vol. 220, p. 112790, Feb. 2024, doi: 10.1016/j.vacuum.2023.112790.
- [39] Y. S. Ho and G. McKay, "Pseudo-second order model for sorption processes," *Process Biochemistry*, vol. 34, no. 5, pp. 451–465, Jul. 1999, doi: 10.1016/S0032-9592(98)00112-5.
- [40] A. E. Rodrigues and C. M. Silva, "What's wrong with Lagergreen pseudo first order model for adsorption kinetics?," *Chemical Engineering Journal*, vol. 306, pp. 1138–1142, Dec. 2016, doi: 10.1016/j.cej.2016.08.055.
- [41] P. Naderi, M. Shirani, A. Semnani, and A. Goli, "Efficient removal of crystal violet from aqueous solutions with Centaurea stem as a novel biodegradable bioadsorbent using response surface methodology and simulated annealing: Kinetic, isotherm and thermodynamic studies," *Ecotoxicol Environ Saf*, vol. 163, pp. 372–381, Nov. 2018, doi: 10.1016/j.ecoenv.2018.07.091.
- [42] L. F. Cusioli, H. B. Quesada, A. T. A. Baptista, R. G. Gomes, and R. Bergamasco, "Soybean hulls as a low-cost biosorbent for removal of methylene blue contaminant," *Environ Prog Sustain Energy*, vol. 39, no. 2, p. e13328, Mar. 2020, doi: 10.1002/EP.13328.
- [43] N. Ali *et al.*, "Organically modified micron-sized vermiculite and silica for efficient removal of Alizarin Red S dye pollutant from aqueous solution," *Environ Technol Innov*, vol. 19, p. 101001, Aug. 2020, doi: 10.1016/j.eti.2020.101001.
- [44] M. B. Gholivand, Y. Yamini, M. Dayeni, S. Seidi, and E. Tahmasebi, "Adsorptive removal of alizarin red-S and alizarin yellow GG from aqueous solutions using polypyrrole-coated magnetic nanoparticles," *J Environ Chem Eng*, vol. 3, no. 1, pp. 529–540, Mar. 2015, doi: 10.1016/j.jece.2015.01.011.
- [45] M. Bellaj *et al.*, "Eco-friendly synthesis of clay-chitosan composite for efficient removal of alizarin red S dye from wastewater: A comprehensive experimental and theoretical investigation," *Environ Res*, vol. 247, p. 118352, Apr. 2024, doi: 10.1016/j.envres.2024.118352.
- [46] G. Bharath Balji and P. Senthil Kumar, "Adsorptive Removal of Alizarin Red S onto Sulfuric Acid-Modified Avocado Seeds: Kinetics, Equilibrium, and Thermodynamic Studies," *Adsorption Science & Technology*, vol. 2022, Jan. 2022, doi: 10.1155/2022/3137870.
- [47] Y. Liu *et al.*, "The adsorption property and mechanism of phenyl/amine end-capped tetraaniline for alizarin red S," *Colloid Polym Sci*, vol. 296, no. 11, pp. 1777–1786, Nov. 2018, doi: 10.1007/s00396-018-4401-0.
- [48] R. K. Gautam, P. K. Gautam, M. C. Chattopadhyaya, and J. D. Pandey, "Adsorption of Alizarin Red S onto Biosorbent of Lantana camara: Kinetic, Equilibrium Modeling and Thermodynamic Studies," *Proceedings of the National Academy of Sciences, India Section A: Physical Sciences*, vol. 84, no. 4, pp. 495–504, Dec. 2014, doi: 10.1007/s40010-014-0154-4.
- [49] M. I. Khamis, T. H. Ibrahim, F. H. Jumean, Z. A. Sara, and B. A. Atallah, "Cyclic Sequential Removal of Alizarin Red S Dye and Cr(VI) Ions Using Wool as a Low-Cost Adsorbent," *Processes 2020, Vol. 8, Page 556*, vol. 8, no. 5, p. 556, May 2020, doi: 10.3390/PR8050556.
- [50] N. F. Attia, S. M. Shaltout, I. A. Salem, A. B. Zaki, M. H. El-Sadek, and M. A. Salem, "Sustainable and smart hybrid nanoporous adsorbent derived biomass as efficient adsorbent for cleaning of wastewater from Alizarin Red dye," *Biomass Conversion and Biorefinery 2022 14:4*, vol. 14, no. 4, pp. 4989–5004, May 2022, doi: 10.1007/S13399-022-02763-Z.

- [51] I. M. Ahmed *et al.*, "Low cost and sustainable biochar-based nanocomposite for the effective remediation of persistent Alizarin Red S," *Int J Environ Anal Chem*, Feb. 2025, doi: 10.1080/03067319.2025.2457107.
- [52] D. R. Rout and H. M. Jena, "Removal of malachite green dye from aqueous solution using reduced graphene oxide as an adsorbent," *Mater Today Proc*, vol. 47, pp. 1173–1182, 2021, doi: 10.1016/j.matpr.2021.03.406.
- [53] H. J. Majeed *et al.*, "Synthesis and application of novel sodium carboxy methyl cellulose-g-poly acrylic acid carbon dots hydrogel nanocomposite (NaCMC-g-PAAc/ CDs) for adsorptive removal of malachite green dye," *Desalination Water Treat*, vol. 320, p. 100822, Oct. 2024, doi: 10.1016/j.dwt.2024.100822.
- [54] A. Makalesi *et al.*, "Adsorption of Malachite Green by An Agricultural Waste: Rice Husk," *dergipark.org.tr*, vol. 8, no. 1, pp. 23–29, 2021, doi: 10.30910/turkjans.749218.
- [55] A. Malhotra *et al.*, "Study of adsorbent characteristics of palm leaves powder as a bio sorbent for removal of malachite green (MG) dye," *Mater Today Proc*, vol. 67, pp. 900–904, Jan. 2022, doi: 10.1016/J.MATPR.2022.07.347.
- [56] R. Mustapha, A. Ali, ... G. S.-... R. in A., and undefined 2021, "Removal of malachite green dye using oil palm empty fruit bunch as a low-cost adsorbent," *researchgate.net*, Accessed: Jul. 29, 2025. [Online]. Available: https://www.researchgate.net/profile/Mohammad-Hakim-Che-
  - Harun/publication/352537618\_Removal\_of\_Malachite\_Green\_Dye\_Using\_Oil\_Palm\_Empty\_Fruit\_Bunch\_as\_a\_Low-Cost\_Adsorbent/links/60cd86ae92851ca3acaf7bba/Removal-of-Malachite-Green-Dye-Using-Oil-Palm-Empty-Fruit-Bunch-as-a-Low-Cost-Adsorbent.pdf
- [57] W.-T. Tsai and H.-R. Chen, "Removal of malachite green from aqueous solution using low-cost chlorella-based biomass," *J Hazard Mater*, vol. 175, no. 1–3, pp. 844–849, Mar. 2010, doi: 10.1016/j.jhazmat.2009.10.087.
- [58] M. Ghaedi, A. Ansari, M. Habibi, A. A.-J. of I. and, and undefined 2014, "Removal of malachite green from aqueous solution by zinc oxide nanoparticle loaded on activated carbon: kinetics and isotherm study," *ElsevierM Ghaedi, A Ansari, MH Habibi, AR AsghariJournal of Industrial and Engineering Chemistry, 2014•Elsevier,* 2013, doi: 10.1016/j.jiec.2013.04.031.
- [59] F. Hemmati, R. Norouzbeigi, F. Sarbisheh, and H. Shayesteh, "Malachite green removal using modified sphagnum peat moss as a low-cost biosorbent: Kinetic, equilibrium and thermodynamic studies," *J Taiwan Inst Chem Eng*, vol. 58, pp. 482–489, Jan. 2016, doi: 10.1016/j.jtice.2015.07.004.
- [60] D. H. A. Sudarni *et al.*, "Malachite Green Removal by Activated Potassium Hydroxide Clove Leaf Agrowaste Biosorbent: Characterization, Kinetic, Isotherm, and Thermodynamic Studies," *https://doi.org/10.1155/2021/1145312*, vol. 2021, Sep. 2021, doi: 10.1155/2021/1145312.
- [61] J. K. Adusei, E. S. Agorku, R. B. Voegborlo, F. K. Ampong, B. Y. Danu, and F. A. Amarh, "Removal of Methyl red in aqueous systems using synthesized NaAlg-g-CHIT/nZVI adsorbent," *Sci Afr*, vol. 17, p. e01273, Sep. 2022, doi: 10.1016/J.SCIAF.2022.E01273.
- [62] P. Adowei, S. Ebong, G. O.-J. of A. S. and, and undefined 2021, "Equilibrium, Kinetic and Thermodynamic Studies of Dyes in Aqueous Solution onto Iron Nanocomposite Stabilized by Irvingia gabonensis Leaf Extract," *ajol.info*, vol. 25, no. 12, pp. 2071–2083, 2021, doi: 10.4314/jasem.v25i12.12.
- [63] T. Santhi, S. Manonmani, T. S.-C. engineering research, and undefined 2010, "Removal of methyl red from aqueous solution by activated carbon prepared from the Annona squmosa seed by adsorption," *rshanthini.com*, vol. 14, pp. 11–18, 2010, doi: 10.3329/cerb.v14i1.3767.
- [64] B. Michalkiewicz, D. Paluch, A. Bazan-Wozniak, R. Wolski, A. Nosal-Wiercí Nska, and R. Pietrzak, "Removal of methyl red from aqueous solution using biochar derived from fennel seeds," *mdpi.comD Paluch, A Bazan-Wozniak, R Wolski, A Nosal-Wiercińska, R PietrzakMolecules, 2023-mdpi.com,* 2023, doi: 10.3390/molecules28237786.